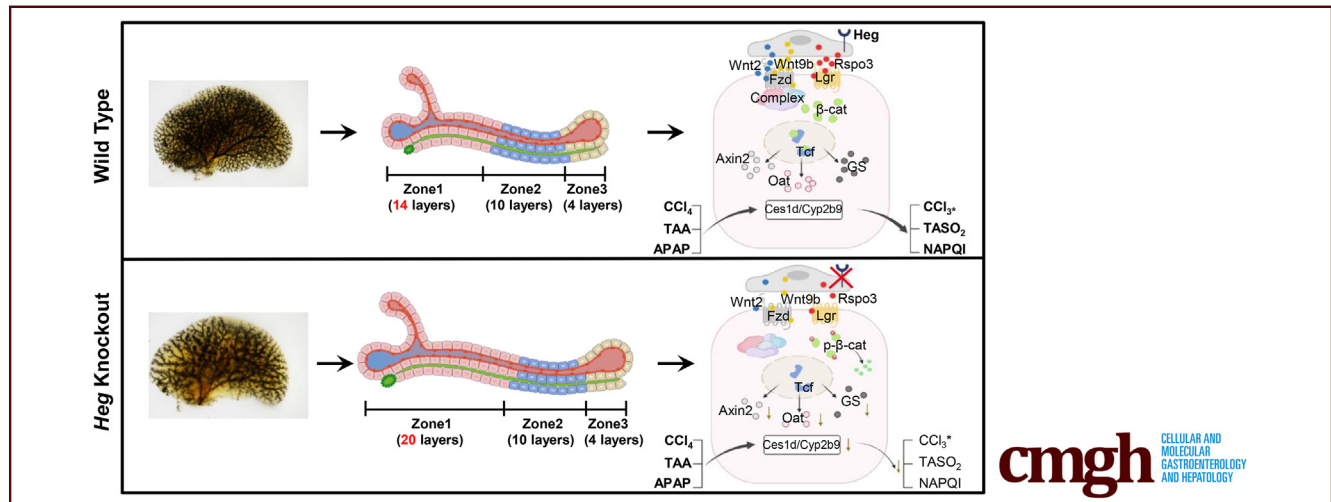


ORIGINAL RESEARCH

Liver Endothelial *Heg* Regulates Vascular/Biliary Network Patterning and Metabolic Zonation Via Wnt Signaling

Shichao Zhu,¹ Xiyun Rao,^{1,*} Yude Qian,^{1,*} Jinbiao Chen,² Renhua Song,³ Huili Yan,¹ Xi Yang,¹ Junhao Hu,⁴ Xiaohong Wang,¹ Zhiming Han,⁵ Yi Zhu,⁶ Renjing Liu,⁷ Justin Jong-Leong Wong,³ Geoffrey W. McCaughan,² and Xiangjian Zheng¹

¹Department of Pharmacology and Tianjin Key Laboratory of Inflammation Biology, School of Basic Medical Sciences, Tianjin Medical University, Tianjin, China; ²Liver Injury and Cancer Program Centenary Institute and Sydney Medical School, The University of Sydney, A.W Morrow Gastroenterology and Liver Center, Royal Prince Alfred Hospital, Sydney, NSW, Australia; ³Epigenetics and RNA Biology Program Centenary Institute and Sydney Medical School, The University of Sydney, Sydney, NSW, Australia; ⁴Interdisciplinary Research Center on Biology and Chemistry, Shanghai Institute of Organic Chemistry, Chinese Academy of Sciences, Shanghai, China; ⁵State Key Laboratory of Stem Cell and Reproductive Biology, Institute of Zoology, Chinese Academy of Sciences, Beijing, China; ⁶Department of Physiology and Pathophysiology, School of Basic Medical Sciences, Tianjin Medical University, Tianjin, China; and ⁷Vascular Epigenetics Laboratory, Victor Chang Cardiac Research Institute, Sydney, NSW, Australia.



SUMMARY

The *Heg* gene in endothelial cells regulates the formation of blood vessel and bile duct networks. Deletion of *Heg* downregulates the expression of drug metabolism enzymes and protects the liver from toxin-induced liver injury.

BACKGROUND & AIMS: The liver has complex interconnecting blood vessel and biliary networks; however, how the vascular and biliary network form and regulate each other and liver function are not well-understood. We aimed to examine the role of *Heg* in mammalian liver development and functional maintenance.

METHODS: Global (*Heg*^{-/-}) or liver endothelial cell (EC)-specific deletion of *Heg* (*Lyve1-Cre;Heg*^{f/f}) mice were used to study the in vivo function of *Heg* in the liver. Carbon-ink anterograde and retrograde injection were used to visualize the 3-dimensional patterning of liver portal and biliary networks, respectively.

RNA sequencing, histology, and molecular and biochemical assays were used to assess liver gene expression, protein distribution, liver injury response, and function.

RESULTS: *Heg* deficiency in liver ECs led to a sparse liver vascular and biliary network. This network paucity does not compromise liver function under baseline conditions but did alter liver zonation. Molecular analysis revealed that endothelial *Heg* deficiency decreased expression of Wnt ligands/agonists including Wnt2, Wnt9b, and Rspo3 in ECs, which limits Axin2 mediated canonical Wnt signaling and the expression of cytochrome P450 enzymes in hepatocytes. Under chemical-induced stressed conditions, *Heg*-deficiency in liver ECs protected mice from drug-induced liver injuries.

CONCLUSION: Our study found that endothelial *Heg* is essential for the 3-D patterning of the liver vascular and indirectly regulates biliary networks and proper liver zonation via its regulation of Wnt ligand production in liver endothelial cells. The endothelial *Heg*-initiated changes of the liver metabolic zonation and metabolic enzyme expression in hepatocytes was functionally

relevant to xenobiotic metabolism and drug induced liver toxicity. (*Cell Mol Gastroenterol Hepatol* 2022;13:1757–1783; <https://doi.org/10.1016/j.jcmgh.2022.02.010>)

Keywords: Heg; Liver injury; Liver Zonation; Wnt.

The liver interwoven vascular and biliary networks are organized as numerous lobules, the functional and structural unit of liver, to perform its diverse functions including nutrient metabolism, detoxification, protein synthesis, and bile secretion.¹ The formation of the 3-dimensional (3-D) network of blood vessels and the biliary system has been closely explored in recent years.^{2–5} Endothelial signaling has been shown to mediate liver development and regeneration,^{6,7} but the molecular regulation of the liver vascular network development is largely unknown. In each lobule, blood flows from the portal tract through sinusoidal vessels to a draining central vein. From the portal vein (PV) to the central vein (CV), hepatocytes can be divided into 3 zones according to the molecular signatures and functional preferences.⁸ A range of factors, such as oxygen tension, metabolic hormone gradient, and angiocrine morphogens, have been implicated to contribute to hepatic zonation.^{9,10} Wnt ligands/agonists including Wnt2, Wnt9b, and Rspo3 produced from pericentral liver endothelial cells (ECs) have been shown to play a dominant role in the establishment and maintenance of hepatic zonation^{6,11–13} However, the upstream signaling component that drives the expression of Wnt ligands in liver ECs is not known.

Biotransformation of xenobiotics is an important step of liver detoxification. The liver contains 2 classes of enzymes essential for the metabolism of xenobiotics. Group I enzymes, including cytochrome P450, flavin-containing monooxygenase, and epoxide hydrolases, catalyze the oxidative and reductive reaction of xenobiotics; and Group II enzymes, including glutathione-S transferase, UDP-glucuronosyltransferase, N-acetyltransferases, and sulfotransferase, catalyze conjugation reactions of metabolites from the group I reaction.^{14,15} These enzymes are also regulated by zonation morphogens and differentially expressed in different hepatic zones. For example, Cyp2e1 is predominantly expressed in pericentral zone 3 and intermediate zone 2 cells, and its expression is positively regulated by Wnt signaling.⁶ Down-regulation of Wnt/ β -Catenin signaling decreases cytochrome P450 expression in zone 3 hepatocytes, and the liver gains resistance from toxic compound-induced injury.^{6,7}

Heart-of-glass (Heg) is a type I transmembrane protein with a large extracellular domain and a relative short, but highly conserved intracellular domain that interact with Krit1 to engage Heg with the cerebral cavernous malformation (CCM) signaling complex.¹⁶ The interaction between Heg and CCM proteins is required for normal heart and vessel development.¹⁶ Heg and *ccm2* have been shown to regulate hepatocyte polarity in zebrafish whereby the loss of Heg or *ccm2* expression causes mis-patterning of the vessel and biliary networks.¹⁷ Here, we demonstrate that deletion of Heg in mouse liver ECs decreased the density of vascular and biliary networks and altered liver metabolic zonation, consequent to

the downregulation of Wnt ligands from endothelial cells. This metabolic zonation change altered the expression level of biotransformation enzymes and protected the liver from hepatotoxin-induced injury. Our data also demonstrated that Heg is an upstream regulator of Wnt ligands that mediated the crosstalk between liver EC and hepatocyte.

Results


Loss Of Heg in Liver Endothelial Cells Decreases the Density of the Liver Vascular Network

Heg has been shown to regulate cardiovascular development.^{16,18} In zebrafish, *heg* deficiency impaired hepatocyte polarity and canaliculi development.¹⁷ To investigate the role of Heg in the mammalian liver, we generated the global *Heg*-deficient (*Heg*^{-/-}) mice. The liver size and weight were comparable between *Heg*^{-/-} and littermate control mice at 3 months of age (**Figure 1A and B**). The level of liver enzymes and bilirubin in plasma were also similar between control and *Heg*^{-/-} mice (**Figure 1C**). Histology analysis revealed no differences except a slight increase of inflammatory cell infiltration in the periportal area of *Heg*^{-/-} liver in (**Figure 1D**). Gene expression analysis revealed a small increase of *Acta2* and *F4/80*, but not other markers of fibrosis and inflammation, in the *Heg*^{-/-} livers compared with those of control littermates (**Figure 1E and F**).

To investigate the potential role of Heg in the development of liver vascular network, we performed the antero-grade injection of Indian ink into the common PV followed by tissue clarification to visualize the vascular network of the portal tract. Vascular branching and density were reduced in *Heg*^{-/-} livers compare to the littermate controls (**Figure 2A and B**). Pecan immunostaining of the liver sections confirmed the decreased vascular density and revealed mis-patterning of the vascular and sinusoid network in the livers of the *Heg*^{-/-} mice (**Figure 2C and D**). Glutamine synthase (GS) staining to label hepatocytes surrounding the CVs further confirmed the reduction in the density of CVs (**Figure 2E**). To quantify the vessel density, we marked the vessels surrounded by GS⁺ cells as CVs and the vessels without GS⁺ cells surrounding as PVs, and found that the densities of the central and portal

*Authors share co-authorship.

Abbreviations used in this paper: 3-D, 3-dimensional; ALB, albumin; ALP, alkaline phosphatase; ALT, alanine aminotransferase; APAP, acetaminophen; AST, aspartate aminotransferase; BDL, bile duct ligation; CCl4, carbon tetrachloride; CCM, cerebral cavernous malformation; CK19, cytokeratin 19; CV, central vein; DBIL, direct bilirubin; ECad, Ecadherin; ECs, endothelial cells; GO, Gene Ontology; GS, glutamine synthetase; GSEA, Gene Set Enrichment Analysis; H&E, hematoxylin and eosin; Heg, heart-of-glass; HUVECs, human umbilical vein endothelial cells; IBIL, indirect bilirubin; PBS, phosphate buffered saline; PV, portal vein; qPCR, quantitative polymerase chain reaction; RNA-seq, RNA-sequencing; TAA, Thioacetamide; TBIL, total bilirubin; TP, total protein; TUNEL, terminal deoxynucleotidyl transferase dUTP nick end labeling.

 Most current article

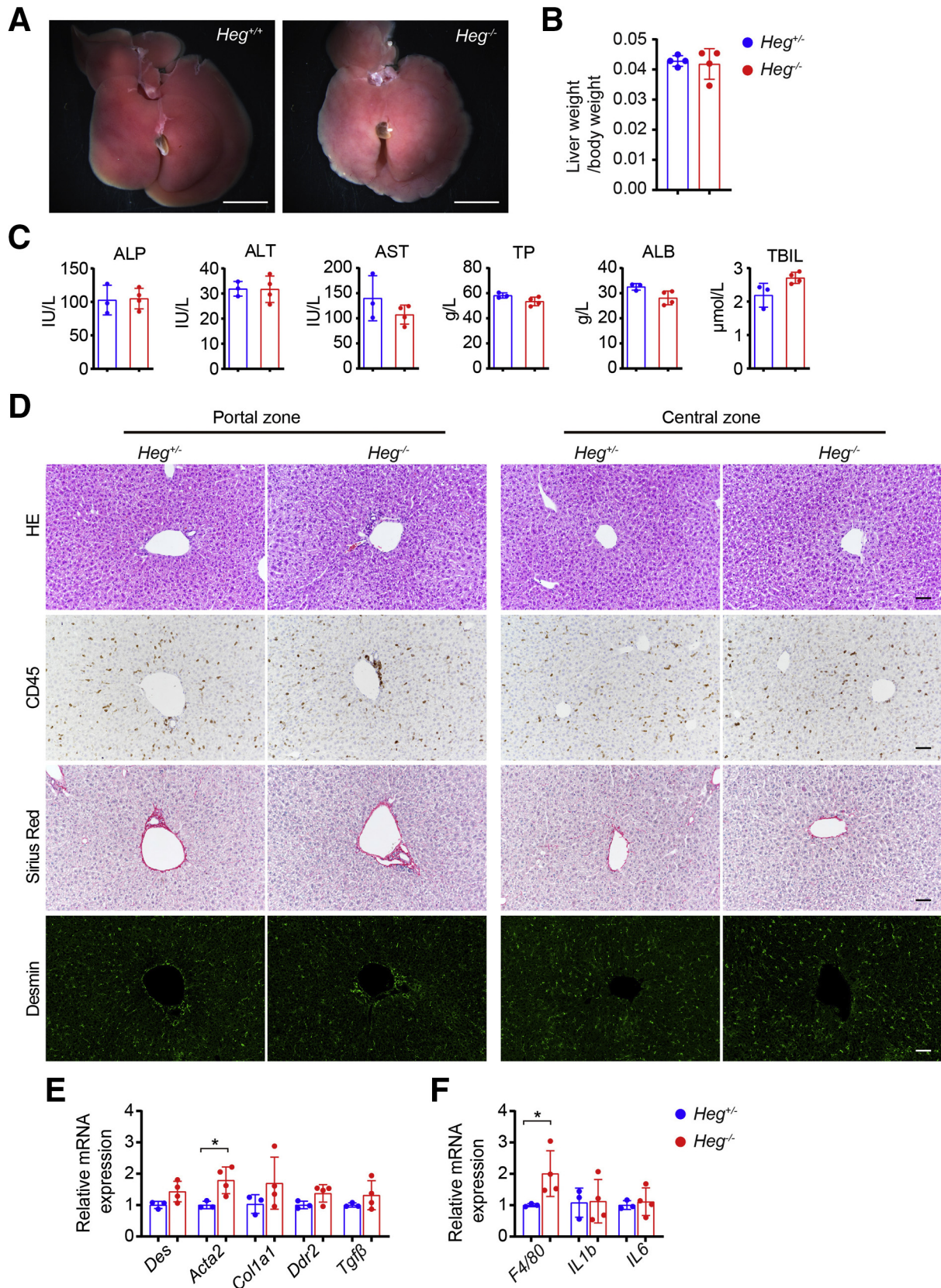
© 2022 The Authors. Published by Elsevier Inc. on behalf of the AGA Institute. This is an open access article under the CC BY-NC-ND license (<http://creativecommons.org/licenses/by-nc-nd/4.0/>).

2352-345X

<https://doi.org/10.1016/j.jcmgh.2022.02.010>

vessels were reduced by 42% and 57% in the *Heg*^{-/-} livers compared with littermate controls, respectively (Figure 2E and F).

Heg is highly expressed in liver ECs, as indicated by gene expression plot from single cell sequencing dataset¹⁹ (Figure 3A) and gene expression analysis of isolated liver



cell groups (Figure 3B). RNAscope analysis indicate *Heg* is highly expressed in ECs of the PVs and sinusoid and CVs, with some expression detected in hepatocytes and epithelial cells of the bile duct (Figure 3C and D). To test whether it is indeed the liver endothelial *Heg* that initiate signaling to regulate the patterning of the vascular network, we generated mice that specifically lack *Heg* in liver ECs by crossing the *Heg^{fl/fl}* mice with the *Lyve1-cre* mice, which express Cre recombinase specifically in the CV and PV and sinusoidal ECs in livers (Figure 3E and F). The exon 1 of the *Heg* gene were flanked with loxP sites in the *Heg^{fl/fl}* mice¹⁶ (Figure 3E). The expression level of *Heg* in liver ECs of the *Lyve1-Cre;Heg^{fl/fl}* (hereafter denoted as *Heg^{LECKO}*) mice was almost absent as assayed with quantitative polymerase chain reaction (qPCR) analysis of samples from livers of embryos at E12.5 and mice at the age of 3 days or 6 weeks (Figure 3G). Similar to the *Heg^{-/-}* mice, no growth defects were observed in the livers of the *Heg^{LECKO}* mice at 2 months of age. 3-D casting of the PV system revealed a dynamic 3-D expansion of the portal vascular network during postnatal development in both the *Heg^{fl/fl}* and the *Heg^{LECKO}* mice, as indicated by the increased density of ink dye in the central areas of liver lobes from ages 4 to 12 weeks. However, it was noted that the *Heg^{LECKO}* livers showed a decreased density of the portal vascular network at all maturation stages compared with *Heg^{fl/fl}* mice (Figure 3H and I). GS immunostaining confirmed the significantly reduced CV and PV density, but the CV/PV ratio was significantly increased in the *Heg^{LECKO}* mice compared with littermate controls (Figure 3J and K). CV lumen coverage area was not affected, whereas the percentage of PV lumen coverage area was significantly increased in the *Heg^{LECKO}* mice (Figure 3K). These data suggest that an expansion of the PV lumen compensated for the reduced PV density in the *Heg^{LECKO}* liver. In addition, the percentage of GS stained area was significantly reduced in the *Heg^{LECKO}* liver (Figure 3K), suggesting that the reduction of pericentral metabolic enzyme capacity was not compensated (Figure 3J and K). Collectively, these results all indicated that endothelial-specific loss of *Heg* significantly reduced the vascular branching in the liver.

Loss of *Heg* in Liver Endothelial Cells Decreases Biliary Network Density

The liver triad consists of PV, bile duct, and hepatic artery. During liver development in mammals, the bile ducts form around the PV following the inductive signaling from PV, whereas the bile ducts guide hepatic artery development.²⁰ We performed the retrograde ink injection into the common bile ducts to visualize the 3-D network of the

biliary network and found the density of the biliary network was also decreased in the *Heg^{LECKO}* livers (Figure 4A and B). Although less branching of the biliary system in the *Heg^{LECKO}* livers was observed, the diameter of the branches of the bile ducts appear to larger in the *Heg^{LECKO}* livers compared with controls (Figure 4A), although we were unable to precisely measure the diameters of comparable grade of bile ducts. The reduction of biliary network density was also confirmed with immunohistochemical staining for cytokeratin 19 (CK19). Interestingly, despite this decrease in overall biliary density, the number of bile ducts for each of the portal tracts was not affected (Figure 4C and D). In addition, no obvious defect of the periportal lymphatic vessels were found in the *Heg^{LECKO}* livers as indicated by stainings of Podoplanin, which is expressed in lymphatic vessels and well-lumenized periportal bile ducts (Figure 4E and F).

Loss of *Heg* in Liver Endothelial Cells Impairs Liver Zonation

Liver lobules are spatially zoned between the portal and central veins. Based on gene expression and metabolic profiles, liver lobule can be divided into three zones: periportal zone (zone 1), intermediate zone (zone 2), and pericentral zone (zone 3). Each zone can be identified with specific biomarkers such as E-Cadherin (ECad) for zone 1, Cyp2e1 for zone 2 and 3, and GS for zone 3. Due to the decreased vascular and biliary density in the livers of the *Heg* deficient mice (Figures 2–4), we hypothesized that *Heg* deficiency may affect liver lobule structure and metabolic zonation. We performed immunostaining of zonation marker proteins to assess zonal distribution. Although GS⁺ and Cyp2e1⁺ cells were comparable between the *Heg^{LECKO}* and control livers, we identified an expanded zone 1 in the *Heg^{LECKO}* liver based on ECad staining (Figure 5A and B). Additionally, the number of cell layers in zone 1 was significantly increased in the *Heg^{LECKO}* livers compared with that in the control livers (from average of 14 layers in the control to 20 layers in the *Heg^{LECKO}* livers). The numbers of cell layers in zone 2 and zone 3 remained the same between the control and *Heg^{LECKO}* livers (Figure 5C–E). The percentage of GS⁺, Cyp2e1⁺, or ECad⁺ cells in each cell layers were comparable between control and knockout mice, with the notable expansion of ECad⁺ in the *Heg^{LECKO}* liver (Figure 5D). Accordingly, the total cell layers of the liver lobules increased to an average 34 layers in the *Heg^{LECKO}* mice compared with an average of 28 layers in control mice (Figure 5E). In each liver lobule, the GS and Cyp2e1 marked zone 3 and zone 2 area remained the same, whereas the area of ECad marked zone 1 increased by ~3 fold in area

Figure 1. (See previous page). *Heg* global knockout does not affect liver function under unchallenged condition. A–B, Micrograph of livers (A) and quantitation of liver/body weight ratio (B) of *Heg^{-/-}* and littermate control mice at 3 months of age (n = 4 per genotype). C, Serum level of liver enzymes (ALP/ALT/AST), protein (TP/ALB), and bilirubin (TBIL) show no significant difference between control and *Heg^{-/-}* mice at 12 weeks of age. D, H&E staining, sirius red staining, immunostaining of CD45 and Desmin. E, mRNA level of liver injury markers (*Col1a1*, *Acta2*, *Desmin*, *Ddr2* and *Tgfβ*). F, mRNA level of macrophage markers (*F4/80*, *Il1β*, and *Il6*). Data are presented as mean ± SD using unpaired Student *t* test. **P* < .05. Scale bars represent 5 mm in panel A and 50 μm in panel B.

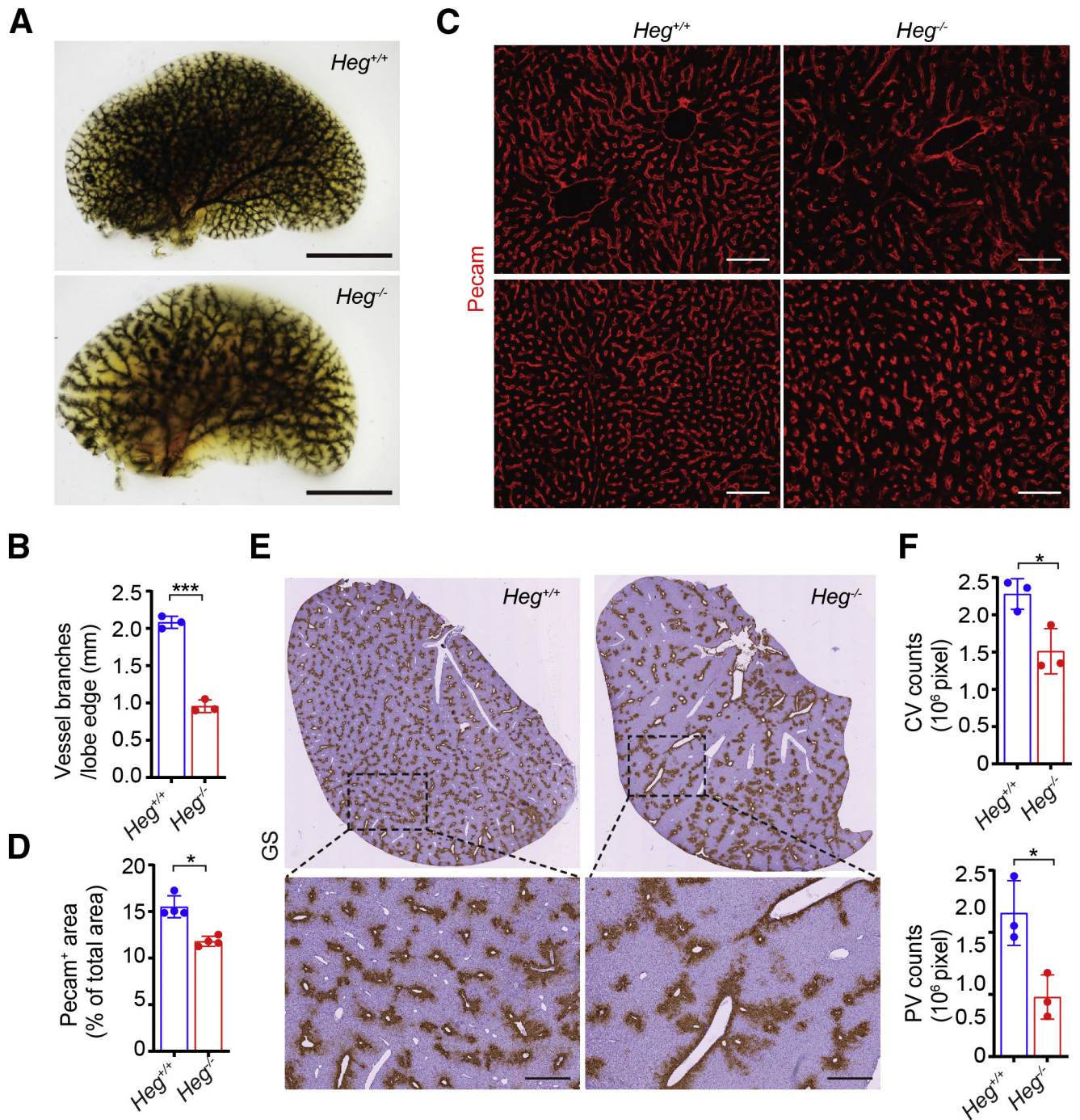


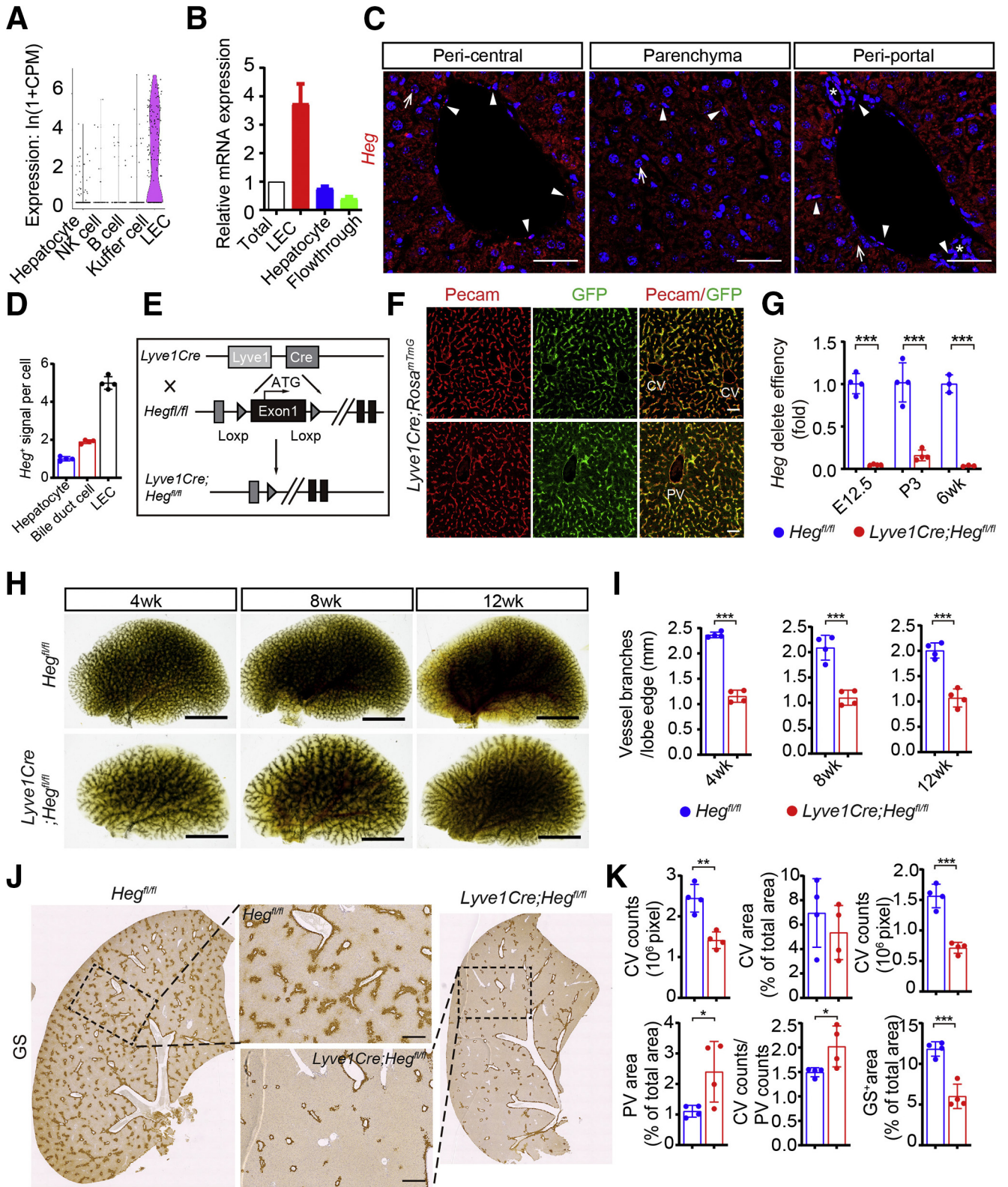
Figure 2. *Heg* deficiency reduces blood vessel density in the liver. A-B, 3-D visualization of portal vein system with anterograde injection of Indian ink (A) and quantitation of peripheral vessel branches (B) to indicate the decreased vessel branching and density in the livers of *Heg*^{-/-} mice at 6 weeks of age. C-D, Pecam staining (C) and quantitation of vessel coverage area (D) of liver sections to indicate the decreased vessel density in the livers of *Heg*^{-/-} mice at 3 months of age. E, GS staining to mark pericentral hepatocytes and the decrease of vessel density in the liver of *Heg*^{-/-} mice at 3 months of age. F, Quantitation plot indicating the decreases of CV and PV density in the liver of *Heg*^{-/-} mice at 3 months of age (n = 4 per genotype). Data are presented as mean ± SD using unpaired *t* test. **P* < .05; ****P* < .001. Scale bars represent 5 mm in panel A, 50 μm in panel C, and 400 μm in panel E.

(Figure 5F). At the whole liver level, there was a significant decrease in the percent of GS⁺ area and no changes to the Cyp2e1⁺ area, and we noted a modest but significant increase in the ECad⁺ area in the *Heg*^{LECKO} mice compared

with controls (Figure 5G). The decreased expression of GS was also observed at the protein levels, and a trend of increasing ECad protein expression was also observed, but quantification did not reach statistical significance

(Figure 5H and I). Gene expression analysis of purified hepatocytes showed decreased expression of zone 3 marker genes (*Axin2*, *Glul*, *Oat*) in the *Heg*-deficient liver compared

with controls, whereas the expression of zone 1 markers (*Cyp2f2*, *Hsd17*, and *Arg1*) remained the same despite an expansion in cell layers in each lobule (Figure 5). Gene



expression analysis of purified liver ECs showed that *Heg* deficiency in ECs altered the expression of certain endothelial zonation genes such that expression of periportal gene *Esm1* was increased and levels of pericentral genes such as *Lhx6* and *Fgfr2* were decreased in the *Heg*^{LECKO} mice (Figure 6A). There was an expansion in *Ace2* expression, a gene predominantly expressed in zone 1 endothelium, coinciding with the expansion of zone 1 in *Heg*^{LECKO} liver (Figure 6B). Immunostaining with Ki67 revealed an increased proliferative activity in zone 1 that was not seen in zones 2 and 3 of maturing *Heg*^{LECKO} liver (3 weeks). Ki67 positive cells were significantly reduced in mature mouse livers (6 weeks), and differences in cellular proliferation between the 2 groups were no longer observed (Figure 6C and F).

Heg Regulates the Expression of Wnt Ligands in Endothelial Cells and Wnt Signaling in Hepatic Cells

To determine how *Heg*, as an endothelial transmembrane receptor, can affect liver lobule patterning and metabolic zonation, we profiled gene expression levels in ECs isolated from control and *Heg*^{LECKO} livers. RNA-seq analysis revealed that Wnt ligands (*Wnt2*, *Wnt9b*, and *Rspo3*) were among the list of top downregulated genes in ECs from the *Heg*^{LECKO} liver (Figure 7A). Gene Ontology (GO) term analysis further confirmed cell-cell signaling by Wnt as one of the top pathways altered in ECs of *Heg*-deficient livers (Fig. 7B and C). *Wnt2*, *Wnt9b*, and *Rspo3* were significantly downregulated in ECs of *Heg*^{LECKO} liver (Figure 7D), and these reductions in Wnt genes were further confirmed in purified liver ECs isolated from the *Heg*^{LECKO} mice (Figure 7E). Wnt ligands are predominantly expressed by ECs of the CV,¹³ and RNAscope analysis demonstrated downregulation of *Wnt2* in ECs of the CV in the *Heg*^{LECKO} mice (Figure 7F and G). Wnt ligands are major angiocrine factors that regulate zonation via canonical signaling in liver parenchymal cells. In the isolated hepatocytes, the expression of known Wnt targets such as *Axin2*, *Glul*, and *Oat*, were significantly downregulated, whereas the expression of Wnt receptors and co-receptors such as *Fzds*, *Lgr4* and *Znf3* were not altered (Figure 7H and I). The expression of β -Catenin mRNA was also not significantly altered in the *Heg*^{LECKO} hepatocytes (Figure 7J). Immunostaining revealed that β -

Catenin protein was predominantly localized to the cytoplasmic membrane of hepatocytes, and its expression levels were similar in pericentral zone 3 and periportal zone 1 hepatocytes of *Heg*^{LECKO} and control livers (Figure 7J). On the other hand, phosphorylated β -Catenin was predominantly found in the cytoplasm, with increased expression observed in the pericentral hepatocytes of the *Heg*^{LECKO} livers (Figure 7K). Expression of phosphorylated β -Catenin was minimum in both the control and *Heg*^{LECKO} peri-portal hepatocytes (Figure 7K). This finding is consistent with previous reports that pericentral ECs are the predominant source of Wnt ligands. Diminished Wnt ligands production promote the increase of phosphorylated β -Catenin and result in the degradation of β -Catenin in pericentral hepatocytes. To further confirm whether *Heg* regulate the expression of Wnt ligands/agonists, we knocked down *HEG* expression with shRNAs in human umbilical vein endothelial cells (HUVECs) that express detectable levels of *RSPO3*, but not *WNT2* and *WNT9b*. Similar to our observations in the *Heg*-deficient ECs, loss of *HEG* levels downregulated the expression of *RSPO3* in HUVECs in vitro (Figure 7L). These results suggest *Heg* is an upstream signal that can positively regulate the expression of Wnt ligands in liver ECs and indirectly maintain canonical Wnt signaling in hepatocytes.

Heg is Required to Maintain Wnt Ligand Expression in Liver Endothelial Cells and Indirectly Regulate Liver Metabolic Zonation

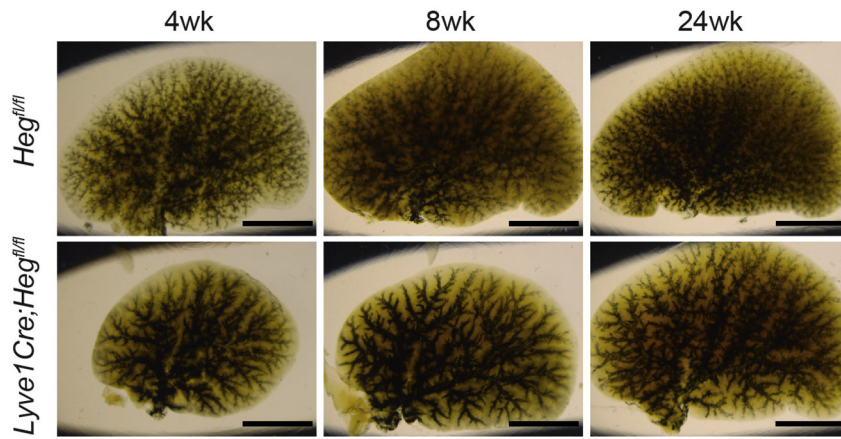
Lyve1-Cre constitutively drives gene deletion from the developmental stage. To test whether it is the developmental defects and vessel density changes indirectly affect Wnt expression or *Heg* regulates Wnt expression in ECs in a cell-autonomous manner, we crossed the *Cdh5-CreERT2* mice with the *Heg*^{fl/fl} mice to generate the *Cdh5-CreERT2;Heg*^{fl/fl} (*Heg*^{iECKO}) and induced *Heg* gene deletion in endothelium after the liver is matured. *Heg* deletion in adult mice for 2 weeks does not change liver vessel density (Figure 8A and B), but can increase the area of zone 1 (ECad⁺) and decrease the area of zone 2/3 (Cyp2e1⁺) (Figure 8C-F). Similar to that of *Heg*^{LECKO} mice, induced deletion of *Heg* also down-regulated the expression of *Wnt2*, *Wnt9b*, and *Rspo3* in liver ECs, and the expression of Wnt target genes, *Axin2*, and *Oat* in

Figure 3. (See previous page). Decrease of liver vascular network density in the *Lyve1-Cre;Heg*^{fl/fl} mice. A, Analysis of single-cell RNA-seq data from Tabula Muris show *Heg* is predominantly expressed in ECs in the liver. B, qPCR analysis of *Heg* expression in isolated liver cells of 6-week-old mice show *Heg* is selectively expressed in ECs. C, RNAscope analysis show *Heg* is expressed (red dots) in ECs, hepatocytes, and epithelial cells of bile duct in livers of mice at age of 6 weeks. D, Quantification of *Heg* RNAscope signal in different liver cell types. E, Schematic of the generation of the *Lyve1-Cre;Heg*^{fl/fl} mice. F, Co-immunostaining of Pecam and GFP on liver section of 3-week-old *Lyve1-Cre; Rosa*^{mTmG} mice show the *Lyve1-Cre* driven recombination in liver ECs including ECs of sinusoid, CVs, and PVs. G, qPCR analysis of *Heg* deletion efficiency in isolated liver ECs from embryo (E12.5), neonatal (P3) and adult (6 week) control and *Lyve1-Cre;Heg*^{fl/fl} mice. H-I, 3-D visualization of PV system with Indian ink injection (H) and quantitation of peripheral vessel branches (I) in the liver of *Lyve1-Cre;Heg*^{fl/fl} and control mice from weaning to adult (4, 8, and 12 weeks of age). J, GS immunostainings indicate the decreased vessel density in the liver of *Lyve1-Cre;Heg*^{fl/fl} mice at 3 months of age. K, Quantitative plots indicate the density and coverage area of CV and PV, and the GS+ areas in the liver of *Lyve1-Cre;Heg*^{fl/fl} and control mice at 3 months of age (n = 4 per genotype). Scale bars represent 5 μ m. Data are presented as mean \pm SD using unpaired *t* test. **P* < .05; ***P* < .01; ****P* < .001. Scale bars represent 50 μ m in panel C and F, 5 mm in panel G, and 400 μ m in panel I.

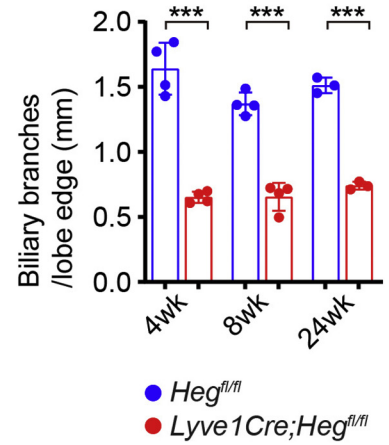
hepatocytes (Figure 8G and H). Together with the phenotype observed in *Heg^{LECKO}* mice, these data suggest *Heg* in liver ECs regulate the development/patterning of

liver vasculature and promote the expression of Wnt ligands, thus, indirectly maintaining appropriate metabolic zonation in the liver.

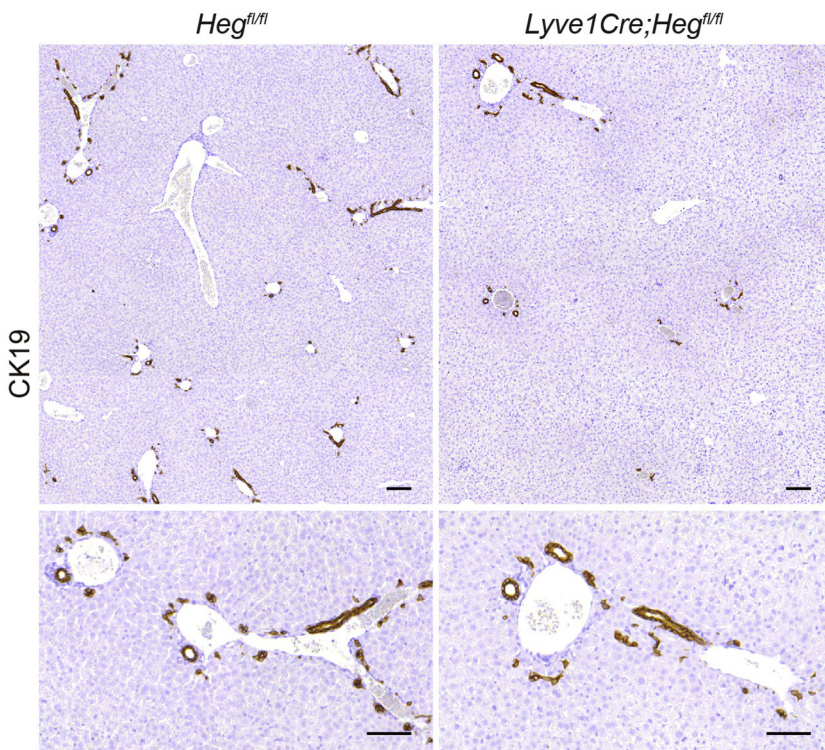
A



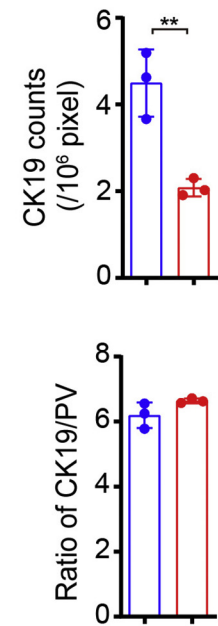
B



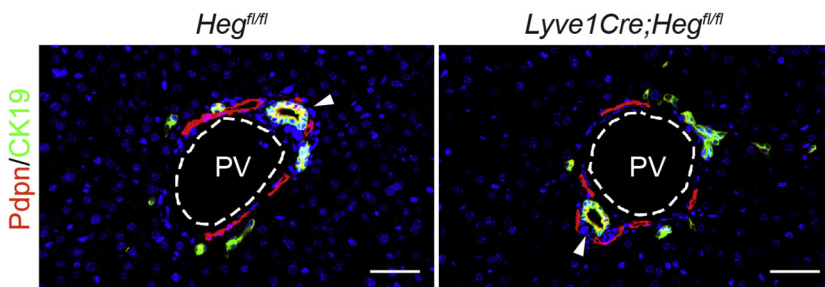
C



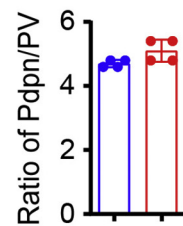
D



E



F



Loss of *Heg* in Liver Endothelial Cells Reduces the Expression of Xenobiotic Biotransformation Enzymes in Hepatocytes

To determine whether the decreased vascular and biliary network density can alter liver zonation and impair liver function, we performed liver chemistry analysis and histology in control and *Heg*^{LECKO} livers. Serum biochemistry analysis revealed no obvious changes of liver enzymes (alkaline phosphatase [ALP], alanine aminotransferase [ALT], and aspartate aminotransferase [AST]), proteins involved in protein synthesis (total protein [TP] and albumin [ALB]), and bile secretion (total bilirubin [TBIL]) between the *Heg*^{LECKO} and control mice (Figure 9A). No notable histological differences, such as lymphocytes infiltration and fibrosis, were detected between control and *Heg*^{LECKO} mice by hematoxylin and eosin (H&E), CD45, Sirius red, and desmin staining (Figure 9B). Gene expression analysis also did not reveal any significant differences in the expression of inflammatory and fibrosis marker genes between the control and *Heg*^{LECKO} livers (Figure 9C and D).

Even though we did not detect an obvious defect in the livers of *Heg*-deficient mice at baseline, we reasoned that *Heg* regulated Wnt signaling might alter the metabolic processes at the molecular level. RNA-seq analysis revealed that differentially expressed genes between control and *Heg*^{LECKO} liver tissues were enriched in drug and chemical metabolism pathways (Figure 10A–C). For example, genes of cytochrome p450 mediated drug metabolism, fatty acid metabolism, and glutathione metabolism were down-regulated in *Heg*-deficient liver (Figure 10D). Among the top genes in the list of differentially expressed genes, *Ces1d*, *Cyp4a14*, and *Cyp2b9* were significantly decreased in the *Heg*^{LECKO} livers (Figure 10E and F).

Loss of *Heg* in Liver Endothelial Cells Prevents Liver From Hepatotoxin-induced Injury

Detoxification is a critical function of the liver to protect the body from chemically induced injuries. Although the *Heg*-deficient livers at baseline were functionally similar to control livers, the observed changes in liver zonation (Figures 5 and 8) and the downregulation of drug metabolizing enzymes (Figure 10) in the *Heg*-deficient mice suggest *Heg* may have a role in regulating liver detoxification. When toxins exceed the liver detoxification capacity, they can induce liver injuries and cause structural and functional damages to the liver.^{21,22} Carbon tetrachloride (CCl₄) is a hepatotoxin widely used to induce liver injury. We treated mice with CCl₄ (1 mL/kg, 3 times a week for 3 weeks) to determine whether *Heg*-deficiency in liver ECs will compromise the toxin handling capability of the liver. CCl₄

treatment led to a significant increase in liver weight in control mice, but this increase was not observed in the *Heg*-deficient mice (Figure 11A). To our surprise, CCl₄ treatment caused less damage to the *Heg*^{LECKO} livers than that of the control livers, as evidenced by reduced sirius red and desmin staining and increased retention of GS⁺ cells in CCl₄-treated *Heg*-deficient liver compared with the CCl₄-treated control livers (Figure 11B–E). These data suggested that the loss of *Heg* in liver ECs protected the liver from CCl₄-induced damage. Further liver function analysis also revealed *Heg*^{LECKO} mice tend to have reduced elevation of ALT and AST levels in response to CCl₄-induced damage (Figure 11F). Similarly, the increases in serum levels of different forms of bilirubin were also less profound in the *Heg*^{LECKO} mice than that of the control mice (Figure 11F). These results together suggest that *Heg*-deficiency in liver ECs was protective against CCl₄-induced liver damage.

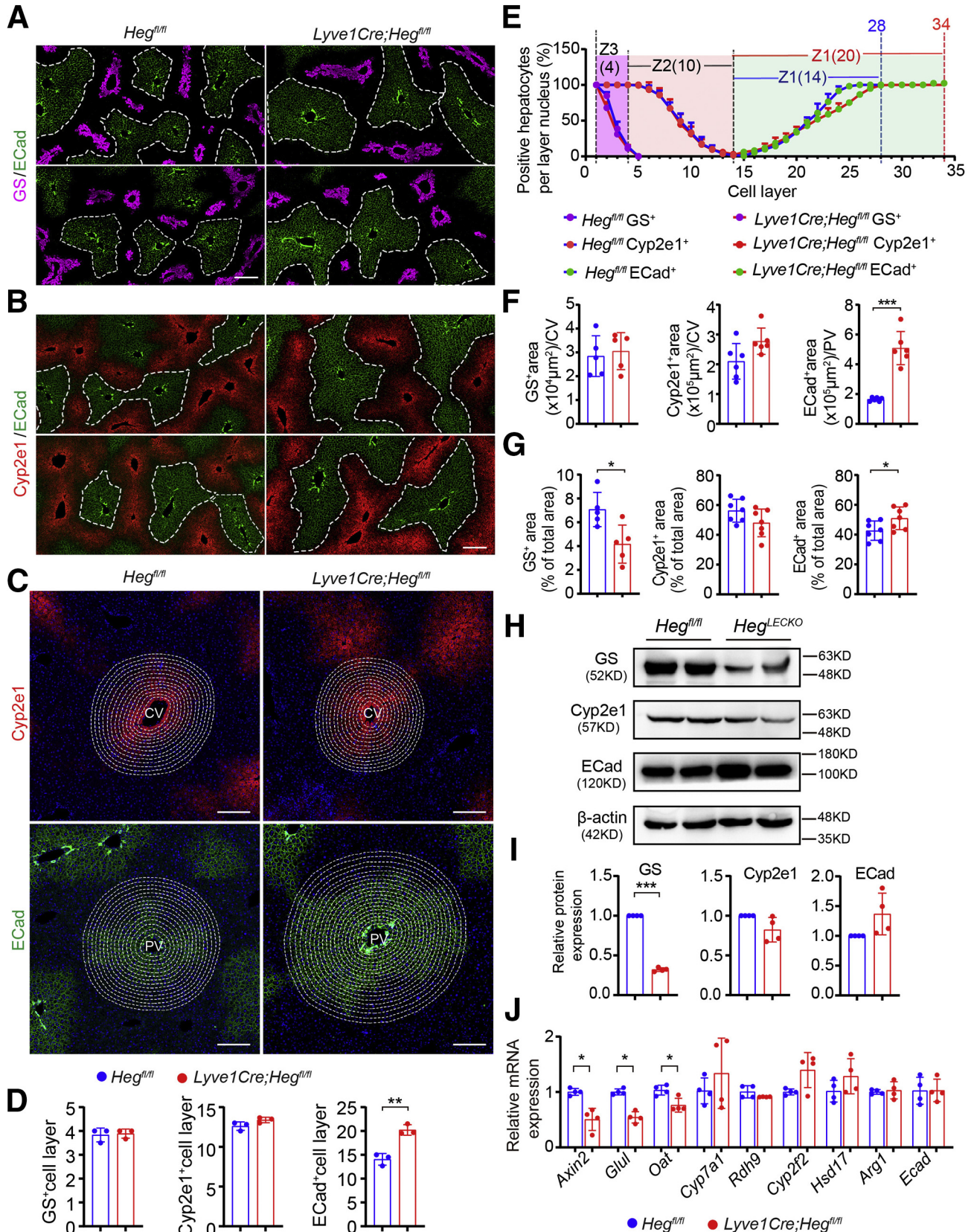
Thioacetamide (TAA) is another toxic chemical used to model chronic liver damage where it is converted to toxic metabolites by Cytochrome P450 enzymes or mono-oxygenases.^{21,23} Treatment with TAA causes compensatory growth of liver and increase of liver weight in control mice (Figure 12A). TAA-induced liver weight gain was significantly diminished in the *Heg*^{LECKO} mice compared with that of littermate controls (Figure 12A). Chronic TAA treatment led to massive infiltration of inflammatory cells to the liver parenchyma in control mice, whereas the number of infiltrated inflammatory cells was significantly less in the TAA-treated livers of the *Heg*^{LECKO} mice (Figure 12B). Similarly, sirius-red staining revealed less fibrosis in the *Heg*^{LECKO} liver. This was further confirmed by reduced expression of collagen and desmin immunostaining in the *Heg*^{LECKO} livers (Figure 12C–D). It is known that TAA causes ductular reaction and immunostaining of CK19 demonstrated severe ductular reaction in the TAA-treated control mice, but this was again decreased in the TAA-treated *Heg*^{LECKO} livers (Figure 12E). qPCR analysis also showed reduced levels of markers for macrophage (*F4/80*), fibrosis (*Col1a1*, *Acta2*, *Desmin*, and *Timp*), and ductal reaction (*CK19*) in the TAA-treated *Heg*^{LECKO} livers (Figure 12F). Consistent with the reduced liver damage as shown by histological analysis, *Heg*-deficient mice also had significantly lower serum levels of ALP and bilirubin in comparison to the control mice after TAA treatment (Figure 12G). These results suggest that *Heg* deficiency in liver ECs protected the liver from TAA-induced liver injury.

To test whether the protective effects to toxin-induced liver injury in *Heg*^{LECKO} liver were specifically due to the down-regulation of xenobiotic biotransforming enzymes, we applied a bile duct ligation model (BDL) that cause liver injury by bile accumulation in liver parenchyma.²² The liver

Figure 4. (See previous page). Decrease of liver biliary network density in the *Lyve1-Cre;Heg*^{fl/fl} mice. A–B, 3-D visualization of biliary network (A) and quantitation of peripheral biliary branches (B) in the liver of *Lyve1-Cre;Heg*^{fl/fl} and control mice at 4, 8 and 24 wk of age. C–D, Immunostaining of CK19 (C) and quantitative plots of total and portal CK19 counts (D) indicating the bile duct density and bile duct/PV ratio in *Lyve1-Cre;Heg*^{fl/fl} and control mice at 3 weeks of age. E–F, Immunostainings of Podoplanin (Pdpn) and CK19 (E) and quantitative plots of the number of Pdpn+ lymphatic vessels (F) show no obvious defect in periportal lymphatic vessels in the liver of *Lyve1-Cre;Heg*^{fl/fl} mice at 8 weeks. ***P* < .01; ****P* < .001; Scale bars represent 5 mm in panel A, 100 μm in panel C, and 50 μm in panel E.

damage in this model is not mediated by cytochrome P450 enzymes or monooxygenase. BDL caused a severe inflammation response and fibrosis from a week after the

procedure. Histology and gene expression changes in 1 to 3 weeks after BDL were similar between *Heg*^{LECKO} mice and its littermate controls (ie, in inflammatory cell infiltration,



the expression of fibrosis makers and duct reaction marker were comparable between *Heg*^{LECKO} mice and its littermate controls (Figure 13). The serum level of liver enzyme and bilirubin also did not differ between *Heg*^{LECKO} mice and its littermate controls (Figure 13J). These results further support our data that a loss of *Heg* in liver ECs was protective against drug-induced injury due to its primary effect on Wnt expression in endothelial cells, indirectly the Wnt-mediated metabolic zonation and the expression of cytochrome P450 enzymes in hepatocytes.

Heg-deficient Mice are Protected From Drug-induced Liver Injury

Acetaminophen overdose is a leading cause of drug-induced liver failure.^{24,25} The expression levels of several reported metabolic enzymes involved in xenobiotic transformation for CCl₄, TAA, and acetaminophen, including (*Ces1d*, *Cyp4a14*, *Cyp2b9*, *Fmo1*, *Fmo5*, and *Ugt1a1*) was significantly down regulated in the *Heg*^{LECKO} livers (Figure 14A and B). To test the effect of *Heg*-regulated xenobiotic transformation pathway in handling injury response to clinically relevant drugs, we administrated *Heg*-deficient and control mice with high doses (300 mg/kg body weight) of acetaminophen. Acetaminophen caused acute liver damage in control mice, 265- and 49-fold increase in plasma ALT and AST, respectively, 24 hours after acetaminophen administration in control mice. Strikingly, only a mild increase in plasma ALT and AST levels were observed in the *Heg*^{LECKO} mice following acetaminophen administration (Figure 14C). It coincided with a significantly reduced number of dead cells in the *Heg*^{LECKO} livers as reflected by H&E and terminal deoxynucleotidyl transferase dUTP nick end labeling (TUNEL) assays (Figure 14D–G). These data further suggest *Heg*-deficiency in ECs can protect the liver from drug-induced liver injury via endothelial cell-hepatocyte communication.

Discussion

In the present study, we have generated a liver EC-specific knockout of the *Heg* that has allowed us to: (1) show that liver endothelial *Heg* signaling regulates vascular and biliary 3-D patterning; (2) identify *Heg* as an upstream regulator of Wnt ligand expression in liver ECs that regulate

liver metabolic zonation; and (3) demonstrate that loss of liver endothelial *Heg* resulted in a decrease in key metabolic enzymes in hepatic zone 3 that protect the liver from drug-induced liver injury.

Although the molecular mechanisms of bile duct morphogenesis in relation to PVs have been extensively studied,²⁰ few studies to date have addressed the regulation of liver vascular and bile duct branch patterning or their interdependence during development and adulthood.^{4,17,26–28} In this study we identified endothelial *Heg* as a key factor in regulating 3-D patterning of the liver vascular and biliary network. Our 3-D visualization of the vascular and biliary networks showed that the loss of *Heg* limited the branching capacity of the vascular network and indirectly reduced the density of the biliary network. The correlated density changes between vascular and biliary networks indicate that vascular patterning guides biliary patterning during network development and maturation. In mammalian liver development, PVs form before bile ducts and induce cholangiocyte specification.^{29,30} The decreased biliary branch density in *Heg*-deficient mice is likely to be a secondary effect caused by a decrease in PV branching, leading to a decrease in actual portal tracks rather than a direct effect of *Heg* on the biliary epithelium. Our results showed that, despite a decrease in portal tracks, the interlobular bile duct per portal track was unaffected and normal. In mice, ECs are essential for liver morphogenesis.³¹ In contrast, the patterning of intrahepatic bile duct systems in zebrafish has been demonstrated as not directly dependent on the vascular network. Liver budding and hepatocyte differentiation progress normally in *cloche* mutant, which lacks endothelial cells.³² However, endothelial *heg* and *ccm2* have been shown to regulate hepatocyte polarity and canaliculi formation,⁴ and a recent study demonstrated that CDK5/Pak/LimK/cofilin in biliary epithelial cell regulated bile duct branching capacity but did not link this to signals from the liver vasculature.¹⁷ Thus, this study showed for the first time that endothelial *Heg* signaling directly modulates the 3-D patterning of vascular networks and then indirectly affects the 3-D patterning of biliary networks in the mammalian liver. The downstream molecular signals that mediate the role of *Heg* in vascular patterning remain to be elucidated.

Figure 5. (See previous page). Deletion of *Heg* in liver ECs alters liver zonation. A–B, Co-immunostainings of zonal markers, GS (zone 3) and E-Cadherin (ECad, zone 1), Cyp2e1 (zone 2/3), and ECad (zone 1) to indicate the zonal distribution within the lobules of *Lyve1-Cre;Heg*^{fl/fl} and control livers at 8 weeks of age. The dash lines mark the edge of ECad⁺ zones. C, Liver sections of control and *Lyve1-Cre;Heg*^{fl/fl} mice at 8 weeks were stained with Cyp2e1 and ECad⁺, example of onion layers of Cyp2e1⁺ hepatocytes and ECad⁺ hepatocytes were marked surrounding CVs and PVs, respectively, Cyp2e1⁺ layers as zone 2, ECad⁺ layers as zone 1. D, Quantitative plots of the average number of GS⁺, Cyp2e1⁺, and ECad⁺ layers in each liver lobules (n = 3 per genotype). E, A continuous plot of the percent of GS⁺, Cyp2e1⁺, and ECad⁺ in each cell layer from pericentral to periportal indicating the increase zone 1 cell layers (from 14 to 20) and total cell layers (from 28 to 34) in each liver lobule in control and *Lyve1-Cre;Heg*^{fl/fl} mice. F, Quantification of GS⁺, Cyp2e1⁺, and ECad⁺ area in each liver lobule. G, Quantification of the percentage of GS⁺, Cyp2e1⁺, and ECad⁺ area in total liver area (n = 5–7 per genotype). H–I, Western blots (H) and quantification (I) of zonation maker, GS, Cyp2e1, and ECad in the whole lysates of livers from 8-week control and *Lyve1-Cre;Heg*^{fl/fl} mice. J, qPCR analysis of the expression level of marker genes of pericentral (*Axin2*, *Glul*, *Oat*, *Cyp7a1*, *Rdh9*) and periportal (*Cyp2f2*, *Hsd17*, *Arg1*, *Ecad*) zones in livers of 8-week control and *Lyve1-Cre;Heg*^{fl/fl} mice (n = 4 per genotype). Data are presented as mean ± SD using unpaired Student *t* test. **P* < .05; ***P* < .01; ****P* < .001. Scale bars represent 200 μm in panel A and B and 150 μm in panel C.

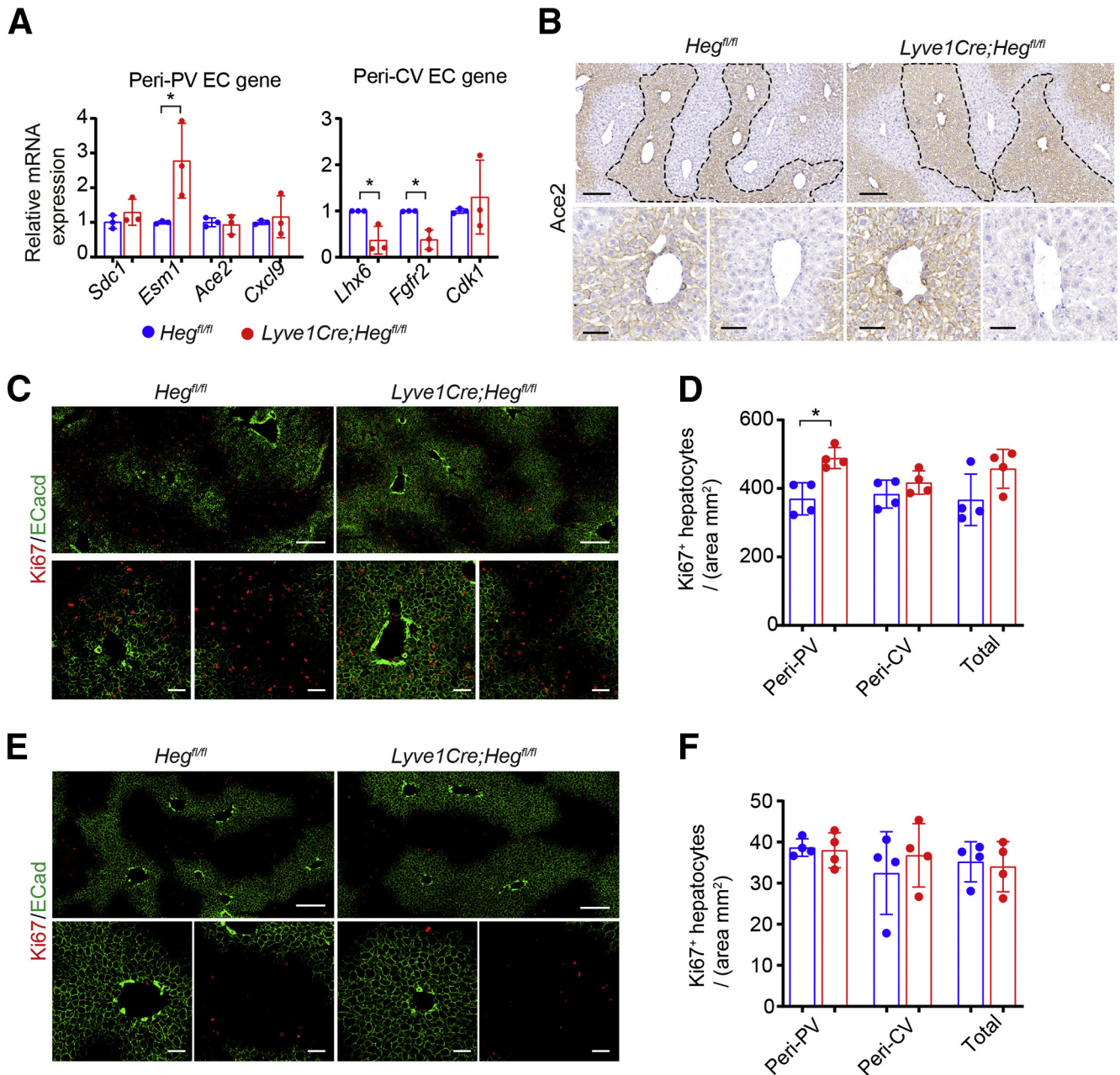


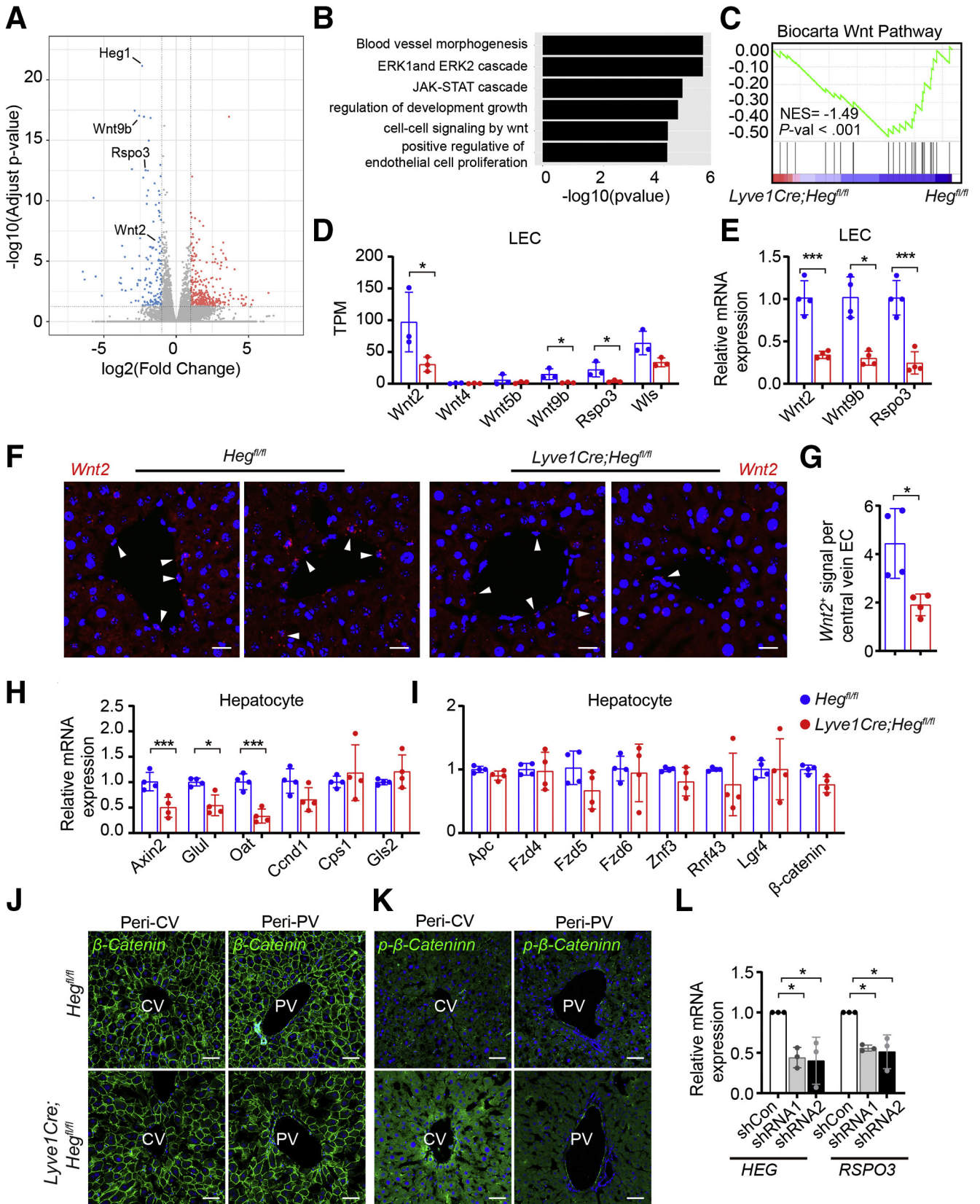
Figure 6. Deletion of *Heg* in liver ECs alters liver endothelial zonation and prompts zone 1 hepatic cell proliferation. A, qPCR analysis of the expression level of marker genes of periportal (*Sdc1*, *Esm1*, *Ace2*, *Cxcl9*) and pericentral (*Lhx6*, *Fgfr2*, *Cdk1*) zone ECs in livers of 8wk control and *Lyve1-Cre;Heg^{fl/fl}* mice (n = 3 per genotype). B, Immunostainings of zonal liver EC marker *Ace2* (zone 1) to indicate LEC zonal distribution within the liver lobules of 8 week control and *Lyve1-Cre;Heg^{fl/fl}* mice. C-F, Co-immunostainings of Ki67/ECadherin and quantitative plots show liver proliferation at different zone in the liver of *Lyve1-Cre;Heg^{fl/fl}* and control mice at 3-week (C and D) and 6-week (E and F) time points. Data are presented as mean \pm SD using unpaired Student *t* test. **P* < .05; ***P* < .01; ****P* < .001. Scale bars represent 200 μ m for top images and 50 μ m for bottom images in panels B, C, and E.

The loss of *Heg* in liver ECs resulting in the decreased expression levels of Wnt ligands is intriguing as the Wnt/ β -catenin signaling is known to be the major regulator of liver zonation.^{33–36} *Wnt2*, *Wnt9b*, and *Rspo3*, are the 3 predominant ligands produced from pericentral ECs to shape liver zonation.^{6,11,37} Deletion of *Rspo3* or blocking Wnt ligands secretion from liver ECs led to the diminished expression of β -catenin target genes such as *Axin2*,

GS, and *Cyp2e1* in the pericentral zone, increased expression of periportal zone genes (*Cyp2f2*, *Hsd17*), and the expansion of the periportal E-cad⁺ zone.^{11,13} Yet, it is not clear what regulates Wnt ligand expression in liver ECs. The molecular and histology phenotypes in our *Heg*-deficient mice closely resemble mice with disrupted Wnt signaling, such as diminished expression of Wnt target genes in pericentral hepatocytes and expansion of

periportal zone. The downregulation of *Wnt2*, *Wnt9b*, and *Rspo3* expression in *Heg*-deficient liver ECs strongly support *Heg* as an upstream positive regulator of Wnt ligand

production in liver ECs, providing an important clue to the regulation and potential environmental stimulation of Wnt expression in liver ECs.



One of our findings related to the structure of the normal liver was the expansion of the number of cell layers for each lobule. Based on zonation marker staining, we observed there was an average of 28 cell layers per lobule in wild-type mice, but that increased to 34 layers in the *Heg*-deficient mice. This was mainly due to the increased layers of E-Cad expressing zone 1 cells, whereas the layers in zones 2 and 3 remained unchanged. A study of the overall numbers of cells in a human liver lobule suggested that a lobule consists of 25 to 30 layers of cells, including 7 to 8 layers of periportal cells and 10 layers of mid-lobular cells.³⁸ The reason for the increase in the layers of ECad⁺ zone1 cells is possibly due to increased hepatocyte proliferation, because we detected increased Ki67⁺ cells in zone 1 of the *Heg*-deficient liver. It may also be due to a lack of Wnt repression signals or be the result of decreased vascular branching activity itself through a yet undefined mechanism. Therefore, how *Heg* regulate liver vascular branching should be a focus of future studies.

Another major finding from this study was the discovery that *Heg* regulated zone 2/3 xenobiotic metabolism. Gene expression data of whole liver tissues revealed significant downregulation of a number of zone 3 metabolic enzymes in the *Heg*-deficient mice, among them *Ces1d*, *Cyp2b9*, and *Cyp4a14*. The effect on the cytochrome P450 system, in association with fatty acid and glutathione metabolism, suggest that *Heg* expression in adjacent ECs indirectly regulate hepatocyte detoxification pathways. This observation was not associated with any changes in liver enzymes, liver immune cells, or extracellular matrix deposition at baseline. It is tempting to link our findings with other studies that have identified the pivotal role of Wnt/ β -catenin signaling in maintaining GS and Cyp450 enzyme expression in pericentral hepatocytes, which are responsible for xenobiotic metabolism.^{6,35,37} Thus, given our findings of a decrease in endothelial cell Wnt ligands, it is not surprising to find that lack of liver endothelial *Heg* expression led to a reduction in hepatocyte xenobiotic metabolism pathways, which reduced the severity of acute liver injuries triggered by CCl₄ and TAA. Our results are also consistent with the finding that liver-specific deletion of β -catenin

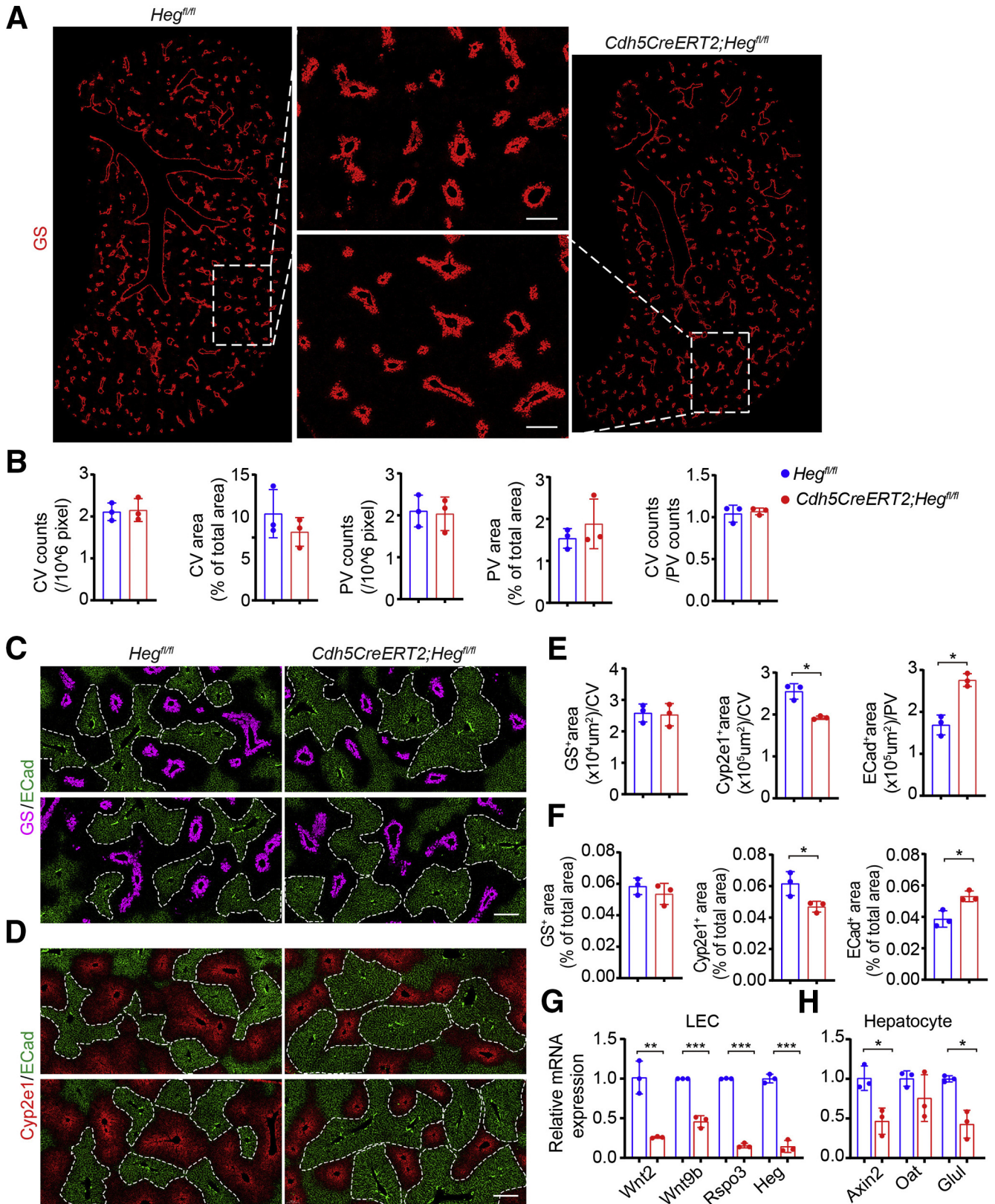
promoted the loss of GS expression in the pericentral hepatocyte, and that ectopic expression of RSPO1 caused an expansion of GS⁺ cells.^{11,39} Therefore, the deletion of *Heg* in liver ECs decreased Wnt ligand production that had the potential to alter zonation, but confer protection for drug-induced liver injuries. However, we are not able to rule out whether the increase in lobule size can alter the oxygen tension and, therefore, its metabolic function. The pathogenic mechanism of CCl₄ and TAA as liver toxins are caused by their conversion to reactive radicals by Cyp450 enzymes to react with nucleic acid, protein, and lipids and cause cell damage.^{21,40} Both CCl₄ and TAA cause damage predominantly in the pericentral zone, although TAA induced a severe ductular reaction, whereas CCl₄ did not. Both CCl₄ and TAA treatment increased the level of ALP, ALT, and AST in the control mice. *Heg* deficiency significantly normalized the elevation of ALT and AST after CCl₄ treatment and prevented ALP upregulation after TAA treatment. In contrast, *Heg* deficiency did not alter liver injury in a bile duct ligation model which does not rely on hepatocyte detoxification mechanisms. This does imply that the protective function of a loss of *Heg* in liver endothelial cells on liver injury is specifically metabolic-related by its indirect regulation of the expression of xenobiotic metabolism enzymes in hepatocytes, but not via the effects of liver endothelial signaling to inflammatory, hepatic stellate, or progenitor cells. The clinical significance of *Heg* regulation of xenobiotic metabolism should be further tested with pharmacological interventions. In this study, we tested the effect of endothelial *Heg* through overdosing with acetaminophen, which causes liver injury via zone 3 metabolic enzymes.^{41,42} Similar to that of CCl₄ and TAA, loss of *Heg* in liver ECs protected the liver from acetaminophen-induced injuries indirectly via altered gene expression in hepatocytes.

Our current study did not show how *Heg* regulates vascular patterning in detail. However, RNA-seq data provided some initial clues for future studies. First, *Heg* was initially identified as an upstream receptor in CCM signaling. It can directly interact with Ccm1 and Rasip1, both of which regulate angiogenesis.^{16,43–45} Thus, *Heg* may function through these proteins and their

Figure 7. (See previous page). Endothelial *Heg* regulates Wnt ligands expression and Wnt/ β -catenin signaling in hepatic cells. A-C, Transcriptomic analysis of liver endothelial cells of *Lyve1-Cre;Heg^{fl/fl}* and littermate control mice at 6 weeks of age. Volcano plot (A) shows *Wnt2*, *Wnt9b*, and *Rspo3* are among the top downregulated genes in *Heg*-deficient liver ECs, GO term analysis (B) and GSEA analysis (C) identified Wnt signaling as a top function that is altered in *Heg*-deficient liver ECs. D, Transcripts per million (TPM) counts of all detectable Wnt ligands and WIs shows *Wnt2*, *WIs*, *Rspo3*, and *Wnt9b* are Wnt signaling genes expressed at high level in liver ECs. E, qPCR analysis confirms *Wnt2*, *Wnt9b*, and *Rspo3* are significantly downregulated in the ECs of *Lyve1-Cre;Heg^{fl/fl}* liver (n = 4 per genotype). F-G, RNAscope analysis and quantification confirm *Wnt2* expression is decreased in the ECs of central veins in livers of 6wk *Lyve1-Cre;Heg^{fl/fl}* mice. H-I, qPCR analysis of the expression of Wnt target genes and Wnt receptor and co-receptor show the downregulation Wnt target genes in purified hepatocytes from 6-week control and *Lyve1-Cre;Heg^{fl/fl}* mice (n = 4 per genotype). J-K, Immunostainings of β -catenin (J) and phosphorylated β -catenin (K) show the constant expression of membrane localizing β -catenin and upregulated phosphorylated β -catenin in livers of 8wk *Heg*-deficient mice. L, qPCR analysis shows the decreased expression of RSPO3 in HUVECs after HEG gene knockdown with shRNA (n = 3 independent repeat experiments). Data are presented as mean \pm SD using unpaired Student *t* test. **P* < .05; ****P* < .001. NS, Not significant.

downstream small GTPase or Notch signaling to regulate vessel patterning in the liver vascular bed, but our RNA-sequencing (RNA seq) analysis of isolated liver ECs and

whole liver tissue did not enrich genes in the Notch signaling. Second, the GO analysis of RNA-seq data identified about a dozen of genes implicated in blood



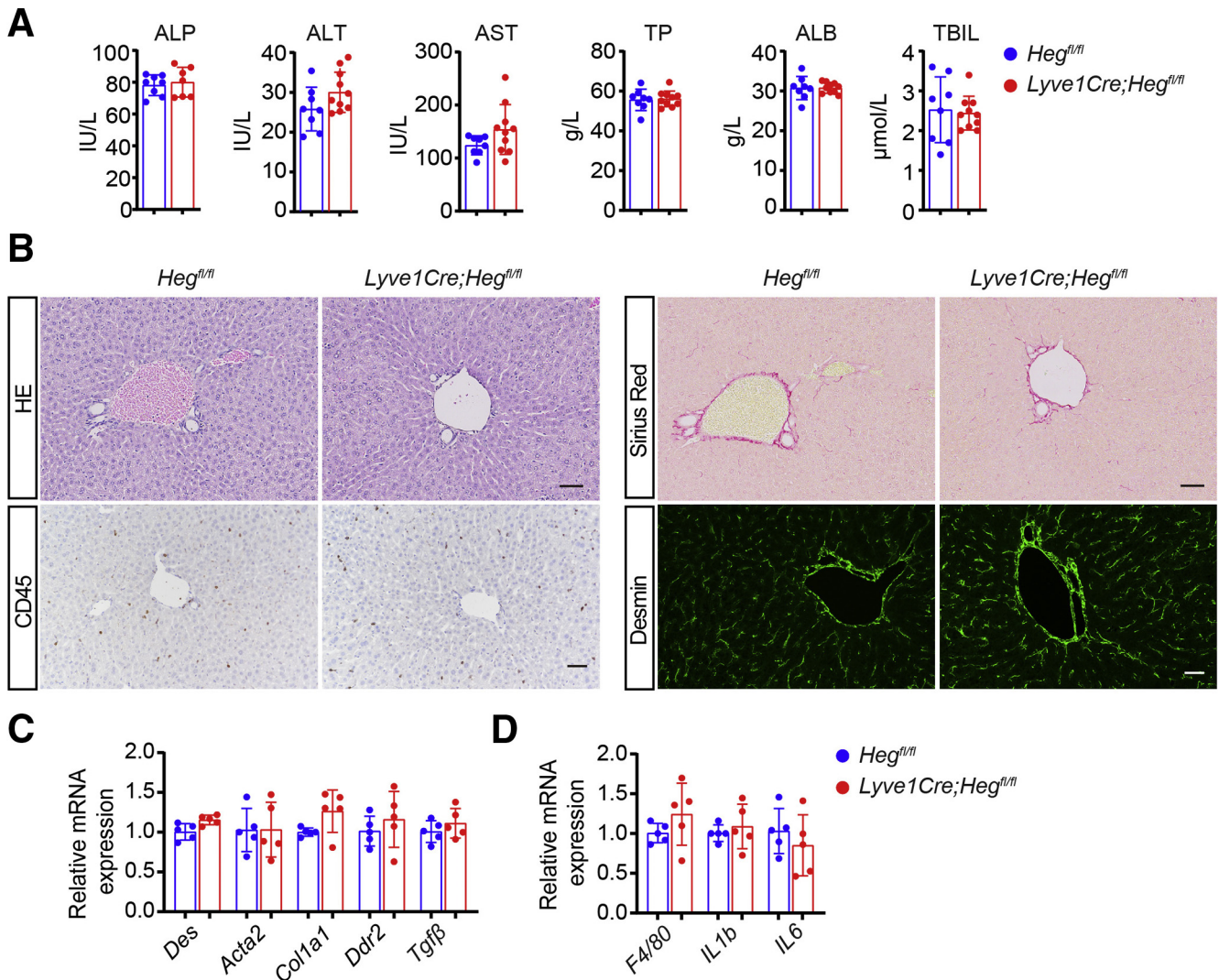


Figure 9. *Heg*-deficiency in liver ECs do not affect liver function under unchallenged condition. **A**, Serum level of liver enzymes (ALP/ALT/AST), ALB, and TBIL show no significant difference between control and *Lyve1-Cre;Heg^{fl/fl}* mice at 12 weeks. **B**, H&E staining, sirius red staining, and immunostaining of Desmin in control and *Lyve1-Cre;Heg^{fl/fl}* liver sections. **C**, mRNA levels of liver injury markers (*Col1a1*, *Acta2*, *Desmin*, *Ddr2*, and *Tgfb*), and **(D)** mRNA level of macrophage markers (*F4/80*, *Il1β*, and *Il6*). Data are presented as mean ± SD using unpaired Student *t* test. Scale bars represent 50 μm.

vessel morphogenesis as the most down-regulated genes in *Heg^{LECKO}* liver ECs such as *Rspo3*, *Cav1*, *Dll1*, *Edn1*, *Bmp4*, and *Bmper*. Among these genes, deletion of *Rspo3* expression with the pan-endothelial cre, *Cdh5-CreERT2*, resulted in reduced vascular density in retina via its regulation of non-canonical Wnt signaling.⁴⁶

Downregulation of Ca^{2+} /Nfat signaling was found to be downstream of *Rspo3* deficiency to cause the decrease of vascular density by regulating vessel pruning.⁴⁶ Whether this *Rspo3*/ Ca^{2+} /Nfat signaling is conserved in the liver and lies downstream of *Heg* to regulate vessel remodeling and density should be investigated. Other proteins, such

Figure 8. (See previous page). Induced deletion of *Heg* in endothelial cells alters liver zonation and Wnt ligands expression. **A**, GS immunostainings indicate no difference of vessel density between livers of 6-week-old control and *Cdh5-CreERT2;Heg^{fl/fl}* mice 2 weeks after tamoxifen induction. **B**, Quantitative plots indicate the density and coverage area of CV and PV in the liver of control and *Cdh5-CreERT2;Heg^{fl/fl}* mice at 6 weeks (*n* = 3 per genotype). **C-D**, Co-immunostainings of zonal markers, GS (zone 3) and ECad (zone 1), *Cyp2e1* (zone 2/3), and ECad (zone 1) to indicate the zonal distribution within the lobules of 6-week control and *Cdh5-CreERT2;Heg^{fl/fl}* mice. The dash lines mark the edge of ECad⁺ zones; scale bars represent 200 μm. **E**, Quantification of GS⁺, *Cyp2e1*⁺, and ECad⁺ area in each liver lobule (*n* = 3 per genotype). **F**, Quantification of the percentage of GS⁺, *Cyp2e1*⁺, and ECad⁺ area in total liver area (*n* = 3 per genotype). **G-H**, qPCR analysis confirms *Wnt2*, *Wnt9b*, *Rspo3*, and *Heg* are significantly downregulated in the liver ECs (**G**) and Wnt targets, *Axin2*, and *Oat* are significantly downregulated in the hepatocytes (**H**) of 6-week *Cdh5-CreERT2;Heg^{fl/fl}* mice (*n* = 3 per genotype). Scale bars represent 50 μm.

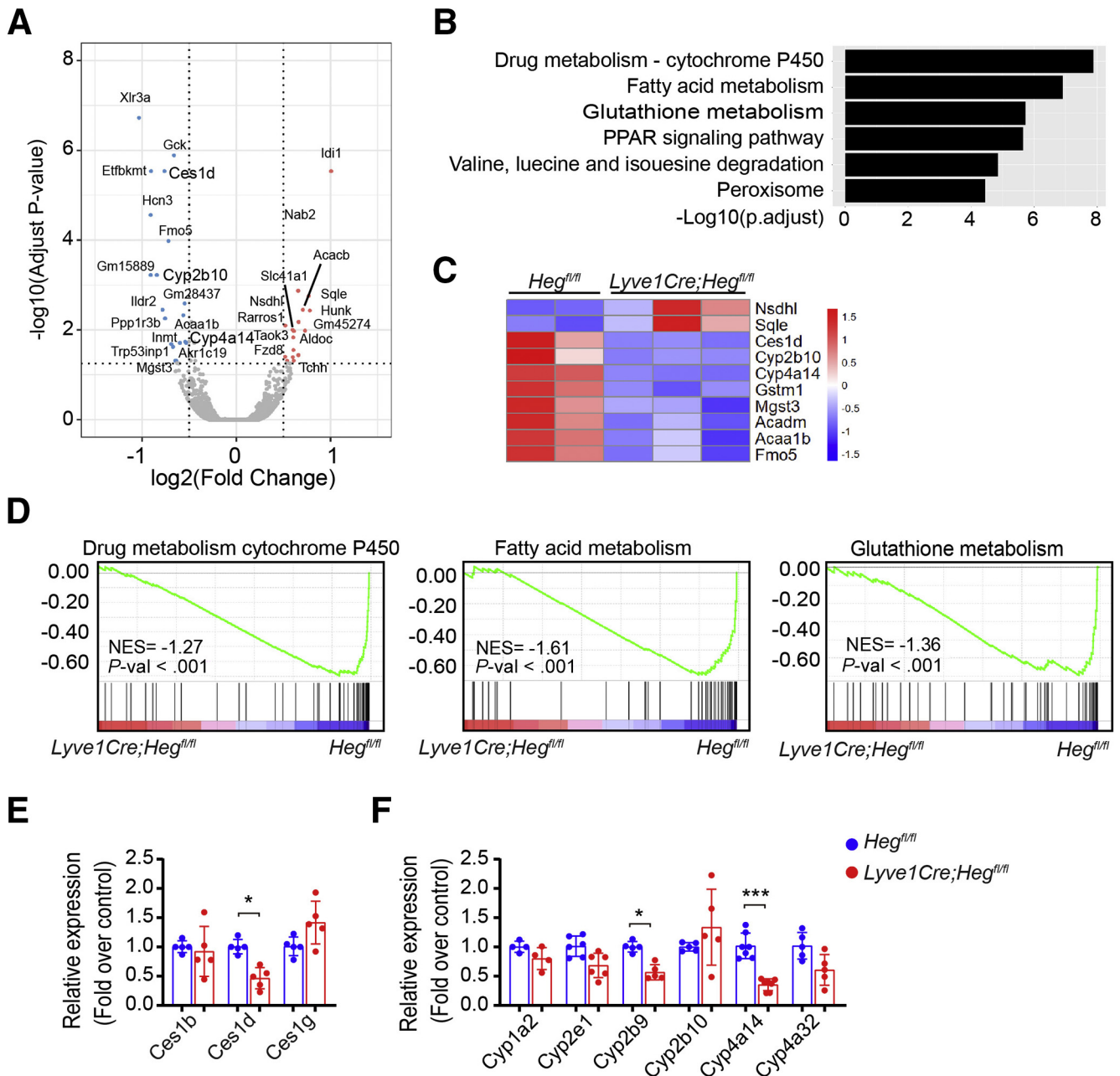


Figure 10. Endothelial *Heg* regulates liver xenobiotic transform enzymes. A, Volcano plot show the DEGs (red, up-regulated genes; green, down-regulated genes) in livers of *Heg*-deficient vs control mice at 12 weeks of age. B, GO term analysis and gene expression heatmap (C) revealed that genes with functions relevant to drug and chemical metabolism pathways are among the top DEGs. D, GSEA analysis shows the gene sets representing metabolism pathways are down-regulated in *Lyve1-Cre;Heg^{fl/fl}* liver. E-F, qPCR analysis show the change of mRNA expression levels of xenobiotic transform enzymes in livers of 12-week *Heg*-deficient mice ($n = 4-6$ per genotype). Data are presented as mean \pm SD using unpaired Student *t* test. * $P < .05$; *** $P < .001$. NS, Not significant.

as BMP4, BMPER, Dll1, Edn1, and Tspan18, have all been shown to promote angiogenesis and vascular patterning.^{47,48} More investigations are required to identify what are the critical downstream signals that mediate the function of *Heg* in regulating liver vascular patterning.

Our finding that *Heg* initiated signaling that regulate vascular/biliary patterning and toxin-induced liver toxicity suggest the possibility that *Heg* may play a role in humans.

Although the predominant *Heg*-expressing cell in the liver at physiological condition is the ECs, a recent study reported *Heg* expression to be increased in liver cancer cell lines and primary liver cancer tissues.⁴⁹ Relevant to our finding that *Heg* is required for Wnt ligand production, *Heg* is found to stabilize β -catenin in these cancer cells and promote cell survival and migration. Further exploration of *Heg* mutations or variants in vascular- or biliary-related human

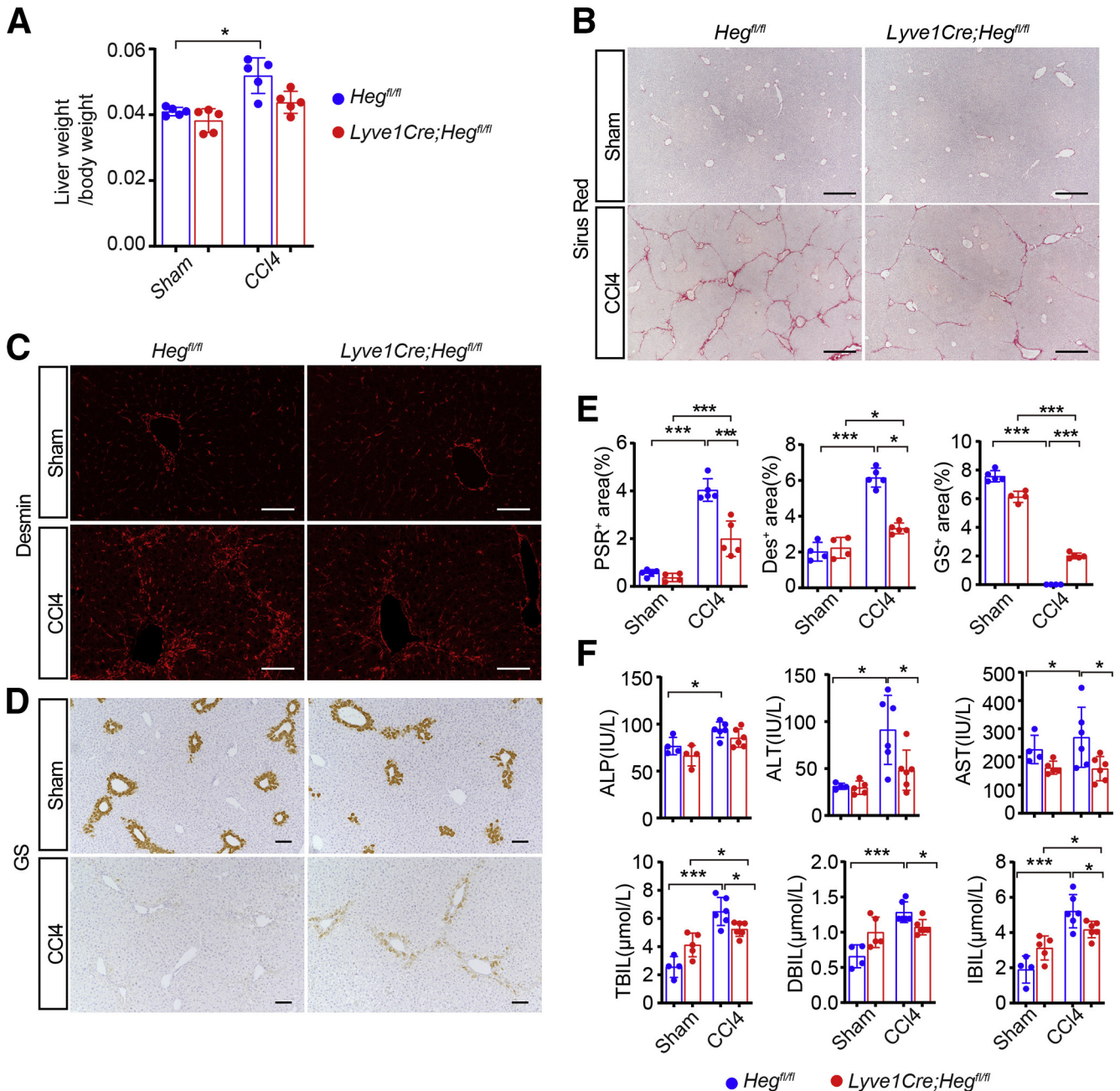


Figure 11. *Heg* deficiency in liver endothelial cells protects the liver from CCl₄ induced injury. A, Ratio of liver weight and body weight show less profound increase of liver weight of 11-week *Lyve1-Cre;Heg^{fl/fl}* mice after 3 weeks CCl₄ treated. B-E, Sirius red staining (B), Desmin staining (C), GS staining (D), and quantification (E) show less severe fibrosis and better pericentral protection in *Lyve1-Cre;Heg^{fl/fl}* mice. F, Serum liver enzyme (ALP/ALT/AST) and bilirubin (TBIL/DBIL/IBIL) levels indicate less damage to liver function in CCl₄ treated *Lyve1-Cre;Heg^{fl/fl}* mice (n = 5 pair for sham group and n = 6 pair for CCl₄ group). Data are presented as mean ± SD using unpaired Student t test. *P < .05; **P < .01; ***P < .001. NS, not significant. Scale bars represent 500 μm in panel B, 100 μm in panels C and D.

liver diseases may point to the clinical significance of *Heg* mediated signaling.

Methods

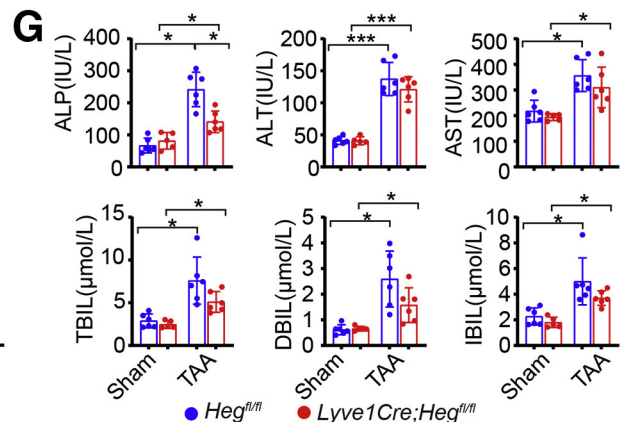
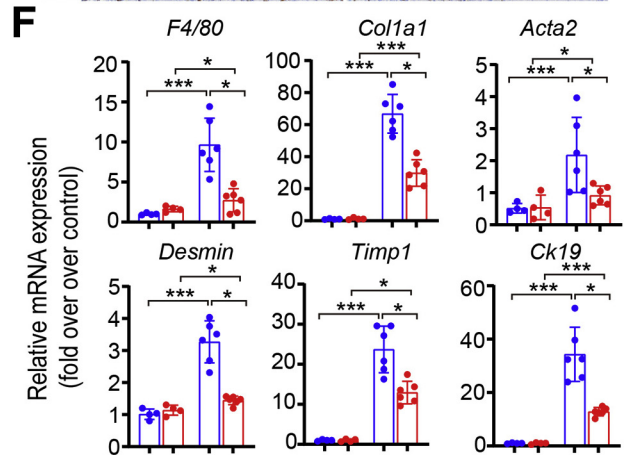
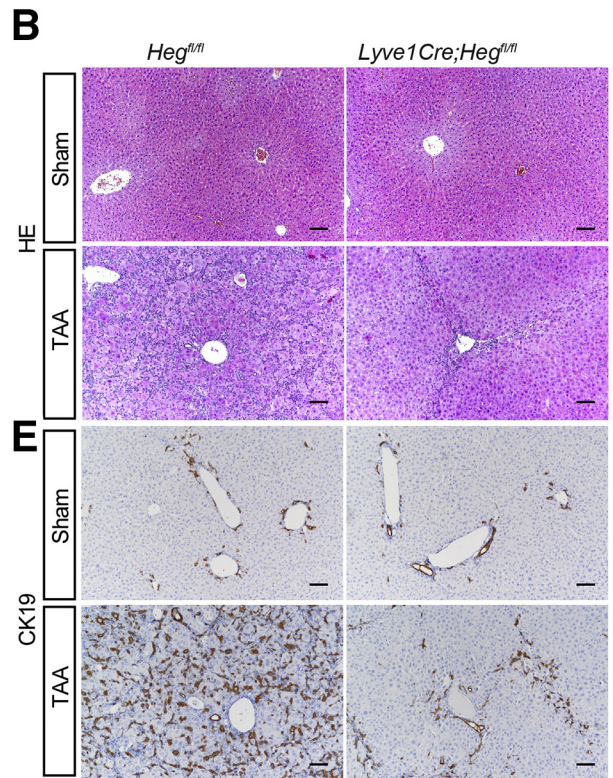
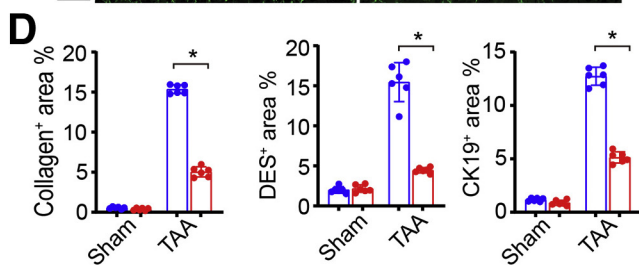
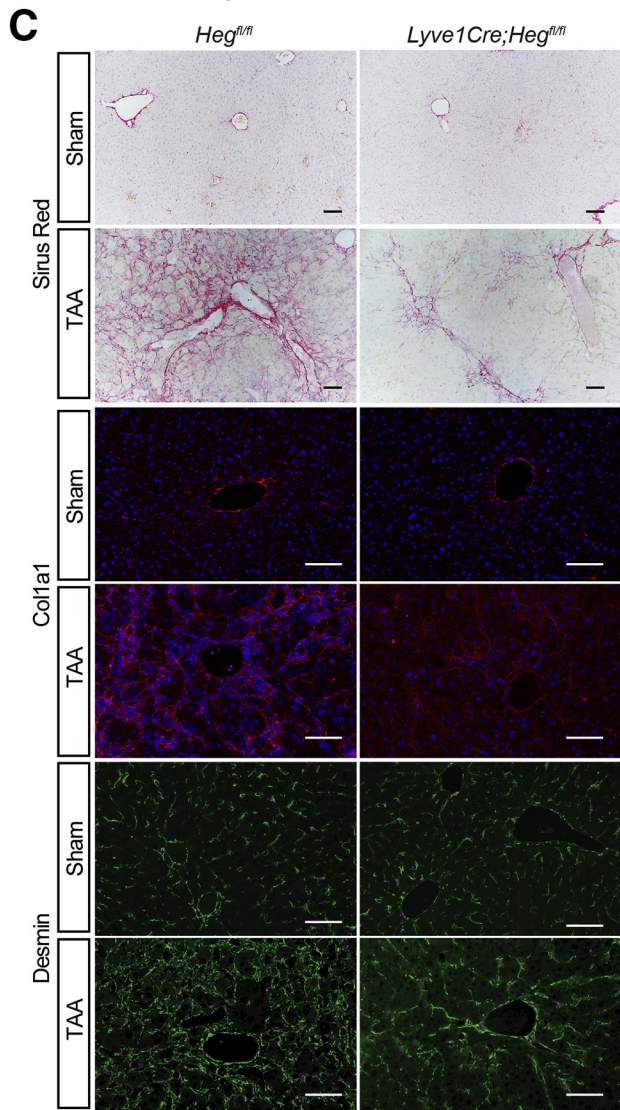
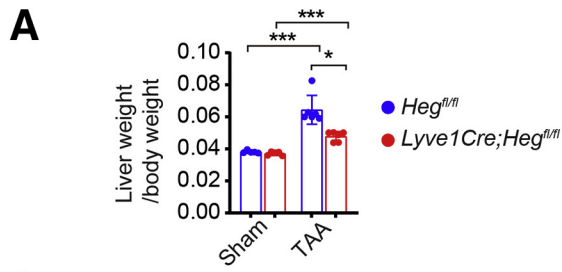
All authors had access to the study data and had reviewed and approved the final manuscript.

Mice

The *Heg^{-/-}* and *Heg^{fl/fl}* mice have been described previously.¹⁶ *Lyve1-Cre*, *Cdh5-CreERT2*, and *Rosa26^{mTmG}* mice were purchased from Jax Laboratories. *Cdh5-CreERT2;Heg^{fl/fl}* mice were given 2 mg tamoxifen per mouse 3 times from 4 weeks of age intraperitoneally. The age- and gender-matched animals were randomized into control and treated groups.

The Institutional Animal Care and Use Committee of Tianjin Medical University and The Sydney Local Health District Animal Welfare Committee approved all animal ethics and

protocols. All experiments were conducted under the guidelines/regulations of Tianjin Medical University, and Centenary Institute, the University of Sydney, the guideline of



National Research Council of the National Academies,⁵⁰ and the Animal Research: Reporting of In Vivo Experiments guidelines.

Visualization of Liver Biliary and Vascular Network

The visualization of the biliary tree was performed according to the protocol developed by Kaneko et al with minor modifications.⁵¹ Briefly, mice were anesthetized and the abdomen was opened to expose the extrahepatic common bile duct. Indian ink (Phygene, PH1714) was slowly infused to the intrahepatic biliary tract by retrograde injection from the extrahepatic bile duct using a 30G needle (Terumo syringe, Japan). The injection was stopped when the ink had reached the surface of the liver. After filling the biliary tree with ink, the liver was harvested and subjected to gradual dehydration with 10 vol%, 40 vol%, and 80 vol% ethanol in phosphate buffered saline (PBS), with each incubation time being 1 hour at RT. The liver was finally incubated in 100% ethanol overnight and then soaked in a 2:1 benzyl benzoate:benzyl alcohol solution. In benzyl benzoate:benzyl alcohol solution, the dehydrated liver becomes optically transparent within a day or two and was then imaged (Nikon, SMZ18 or Leica, M165FC).

For the visualization of the liver vascular network, similar procedures were performed for the biliary tree, except the ink was slowly infused to the liver vessels by injection from the portal vein using a 30G needle. The injection was stopped just before the ink reached the liver lobe edge. Tissues were processed and imaged as above.

The vascular and biliary densities were represented by branches of peripheral ink-filled blood or bile duct per mm of lobe edges of the livers.

Immunofluorescence and Immunohistochemistry

After dewaxing and hydration, tissue sections were boiled in 10 mM citrate buffer solution (pH 6.0) for antigen retrieval, then blocked with 10% donkey serum at room temperature, incubated with appropriate primary antibodies overnight at 4°C. For immunohistochemistry, sections were incubated with horseradish peroxidase-conjugated secondary antibodies, then developed using 3,3'-Diaminobenzidine (DAB) tablet (Sigma), counterstained with hematoxylin. For immunofluorescence staining, sections were incubated with fluorescence-conjugated secondary antibodies for 1 hour at room temperature, then counterstained with 4, 6-diamidino-2-phenylindole (DAPI, Solarbio, China) and images were acquired under

a fluorescence microscope. The following primary antibodies were used: anti-desmin (Abcam, ab15200, 1:300 dilution), anti-Col1a1 (ABclonal, A16891, 1:300 dilution), anti-Ck19 (Abcam, ab133496, 1:300 dilution), anti-GS (Abcam, ab49873, 1:5000 dilution), anti-Cyp2e1 (Atlas, HPA009128, 1:200 dilution), anti-Ecad (BD, BD610181, 1:300 dilution), anti-CD31 (Dianova, DIA-310, 1:300 dilution), anti-GFP (CST, 2555s, 1:300 dilution), anti- β -catenin (Santa, SC-7963, 1:300 dilution), anti-p- β -catenin (SC-57535, 1:200 dilution), Ace2 (Santa, SC-390851, 1:100 dilution), PDPN (Abcam, ab256559, 1:500 dilution), Ki67 (Abcam, ab15580, 1:300 dilution).

Immunoblot Analysis

Whole liver tissue homogenates were prepared in RIPA buffer (150 mM NaCl, 1% NP-40, 50 mM Tris [pH 8.0]) containing protease inhibitors. Protein concentrations of the homogenates were determined by BCA (Thermo Fisher Scientific, 23252). Protein was separated by electrophoresis using SDS-polyacrylamide gel and transferred to polyvinylidene difluoride membranes. The membranes were blocked with 5% skim milk and probed with primary antibodies anti-GS (Abcam, ab49873, 1:5000 dilution), anti-Cyp2e1 (Atlas, HPA009128, 1:1000 dilution), anti-Ecad (BD, BD610181, 1:1000 dilution) overnight at 4°C and followed with the incubation of respective peroxidase-conjugated secondary antibodies for one hour at room temperature. Blots were developed with ECL Western Blotting Substrate (Thermo Fisher Scientific), and the signals were acquired with MiniChem610 (Beijing Sage Creation Science Co Ltd) in dark field mode and marker merged mode.

Quantification of Liver Central and Portal Vein Counts and Area

Slides were stained with peri-CV hepatocytes marker (GS), scanned with Panoramic MIDI (3D HISTECH, Hungary). Images were exported from Panoramic Scanner, then import to Image J (version 1.48). According to the image ruler, set "Distance in pixels" to 100, "known distance" to 100 μ m. Central and portal veins were marked with "wand tool"; liver areas were calculated.

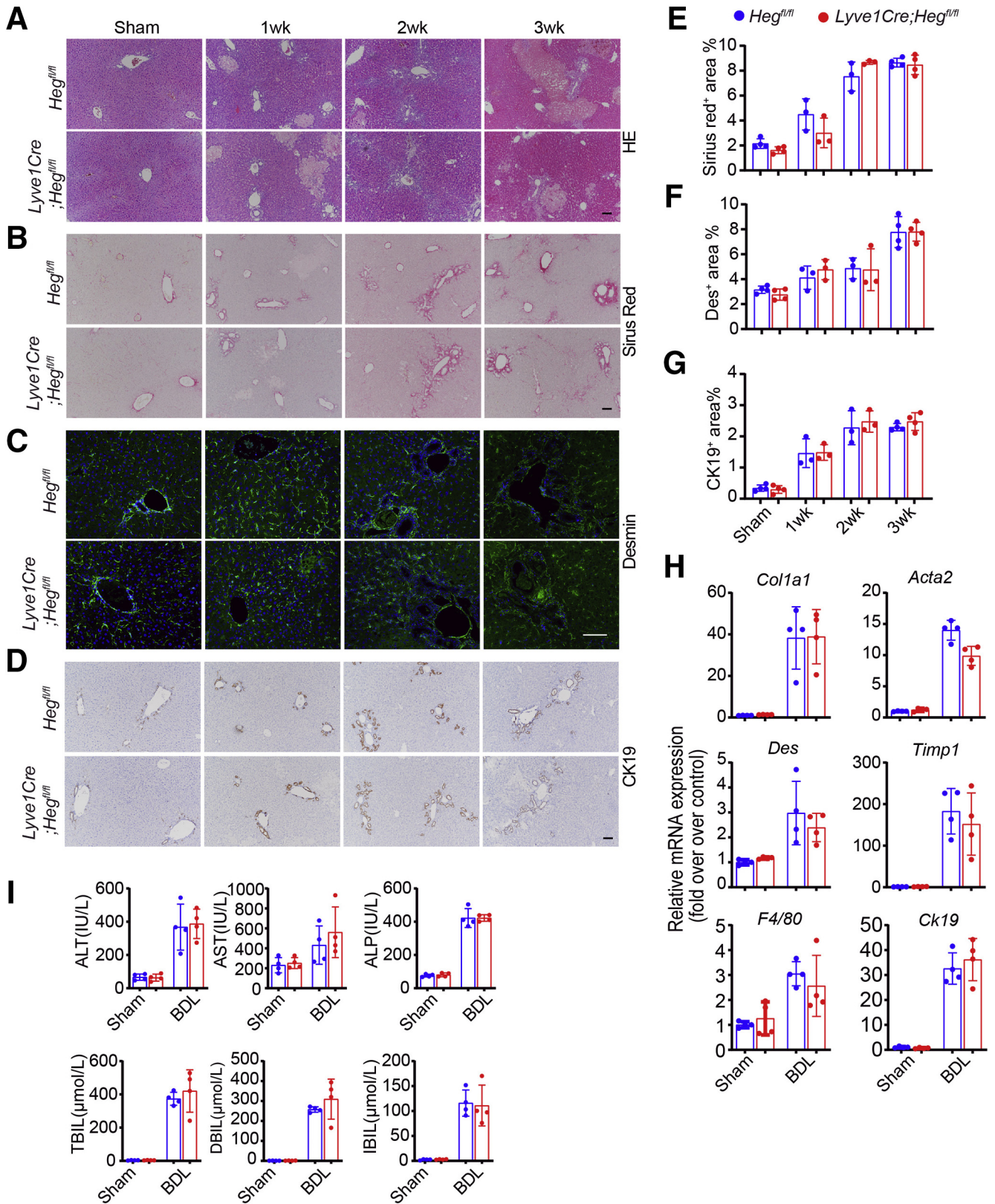
Quantification of Liver Lobule Cell Layers

Liver sections were immunostained with GS, Cyp2e1 or Ecad to mark zone 3, zone 3/2, and zone 1 regions in the liver, respectively. Cell layer were manually marked

Figure 12. (See previous page). *Heg* deficiency in liver endothelial cells protects the liver from TAA induced injury. A, Ratio of liver weight over body weight show less profound compensatory liver weigh growth of 16wk *Lyve1-Cre;Heg^{fl/fl}* mice after 8 weeks TAA treated. B-F, H&E staining (B), Sirius red, Col1a1, and Desmin staining (C), quantification (D), CK19 staining (E), and qPCR analysis (F) of marker genes show less lymphocyte infiltration, less fibrosis, and milder ductal reaction in TAA treated *Lyve1-Cre;Heg^{fl/fl}* mice. G, Serum liver enzyme analysis (ALP/ALT/AST) and bilirubin (TBIL/DBIL/IBIL) indicate less damage to liver function in CCl4 treated *Lyve1-Cre;Heg^{fl/fl}* mice. Data are presented as mean \pm SD using unpaired Student *t* test (*n* = 6 pair for sham group and *n* = 6 pair for TAA group). **P* < .05; ***P* < .01; ****P* < .001. NS, not significant. Scale bars represent 100 μ m in panels B, C, and E.

according to the shape of PV or CV and nucleus of hepatocytes (DAPI labeled). The percentage of GS⁺, Cyp2E1⁺, or Ecad⁺ cell in each layer were calculated (Figure 5). The

average number of cell layers for each zone were calculated from liver sections of 3 mice, and 10 sample image fields with similar CV or PV size were assessed for each liver.



Isolation of Liver Endothelial Cells and Hepatocytes

Liver ECs and hepatocytes were isolated as described with minor modifications.⁵² Briefly, mice were anesthetized with avertin and perfused with D-Hanks through the portal vein, followed by perfusion with Hanks buffer containing 0.2 mg/mL of collagenase intravenously (Sigma-Aldrich, C5138). The liver was removed and placed in Hank's buffer with gently agitation, and the cell suspensions were filtered through a 70 μ m nylon mesh, centrifuged at 68 g for 5 minutes at 4 °C. The precipitations contain mostly hepatocytes. The supernatant was further centrifuged at 350 g for 5 minutes. The cell pellets were resuspended with Macks Buffer (D-Hanks + 0.5% BSA+2 mM EDTA). Liver EC were then isolated by magnetic-activated cell sorting using anti-CD31 MicroBeads (Miltenyi Biotech, Germany) according to the manufacturers' instructions. The purity of liver EC was confirmed by qPCR compared with whole liver, hepatocytes, supernatants, and flow-through using different cell markers.

RNA Extraction, Reverse Transcription, and qPCR Analysis

Total RNA was extracted from tissue or cell homogenates using Trizol reagent (Invitrogen) and cDNA was synthesized from 1 μ g of total RNA by reverse transcription (GeneStar, China). qPCRs were performed using SYBR QPCR Master Mix (Vazyme), and the primer pairs used are listed at the end of this section. The level of target gene expression was normalized to GAPDH expression in each sample.

RNA Sequencing

Total RNA was isolated from total liver tissue or liver ECs of control and *Lyve1-Cre;Heg^{fl/fl}* mice. Only high-quality RNA sample with OD260/280=1.8~2.2, OD260/230 \geq 2.0, RIN \geq 7, 28S:18S \geq 1.0 were used for sequencing library construction. Paired-end RNA-seq sequencing library was sequenced with the Illumina HiSeq xten/NovaSeq 6000 sequencer (2 \times 150 bp read length) (majorbio, China). All clean reads were separately aligned to reference genome with orientation mode using HISAT2 (<http://ccb.jhu.edu/software/hisat2/index.shtml>) software. The mapped reads of each sample were assembled by StringTie (<https://ccb.jhu.edu/software/stringtie/index.shtml?t=example>) in a reference-based approach.⁵³ To identify DEGs (differential expression genes) between 2 different samples, the expression level of each transcript was calculated according to the transcripts per million reads method. Differential

expression analysis was performed using the DESeq2. Genes with Q value \leq 0.05, DEGs with $|\log_2FC| > 1$ and Q value \leq 0.05 (DESeq2) were considered to be significantly different expressed genes. In addition, GO functional-enrichment analysis was performed to identify which DEGs were significantly enriched in GO terms and metabolic pathways at Bonferroni-corrected *P*-value \leq .05 compared with the whole-transcriptome as background. Gene Set Enrichment Analysis (GSEA) was implemented on the R (version 3.6.1). Gene sets with nominal *P* values less than .05 were considered statistically significant.

RNAscope in situ Hybridization

After deparaffinized in xylene, rehydrated in ethanol, and tissue sections were processed for RNA in situ hybridization using the RNAscope LS Multiplex Fluorescent Reagent Kit following the manufacturer's instructions (Advanced Cell Diagnostics). The *Wnt2* (Mm-Wnt2, Cat. 313601, NM_023653.5, region 857-2086) and *Heg* (Mm-Heg1-C2, Cat. 510581-C2, NM_175256.5, region 1927-2856) RNA-scope probe were used. Sections were counterstained with DAPI and mounted. Positive RNAscope signals were quantified in Image J software, the expression levels of *Wnt2* or *Heg* were presented as number of signals per cell of the specified liver cell type.

In vitro Knockdown of HEG

For in vitro knockdown of *HEG* in HUVEC, shRNA of human *HEG* and control nonsense shRNA were purchased from Vigene Bioscience (China). psPAX2, pMD2, and shRNA plasmids were transfected into HEK293T using PEI, 8 hours post-transfection, the medium was removed from the transfected cells and replaced with fresh medium. Virus was harvested from the HEK 293T cells 48 hours and 72 hours post-transfection, and concentrated with 40% PEG8000, store at -80 °C. To knock down of *HEG* in vitro, the lentiviral vectors were added to the culture media of HUVEC. The sequences of the shRNA are *HEG*-shRNA-1, 5'-CCGAG-CATGTGAAGATGGATATAG-3';

HEG-shRNA-2, 5'-ACCTTCGTGACAGAGTTTAAA-3'.

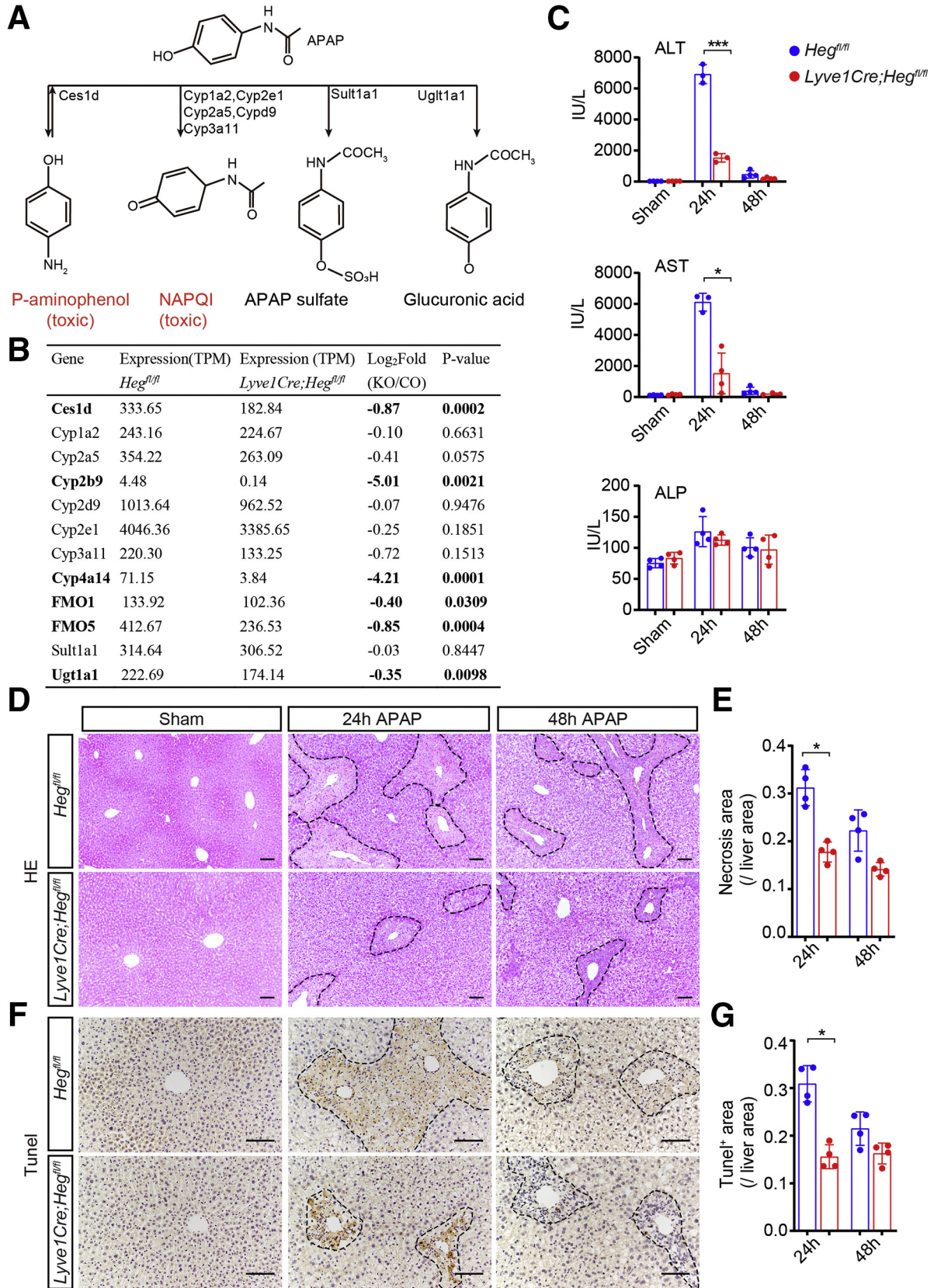
Liver Injury Models

For the CCl₄ induced liver injury model, 8-week old male littermate mice were given with 1 mL/kg CCl₄ (Rhawn, China, mixed with corn oil at a ratio of 1:4) via intraperitoneal injection 3 times a week for 3 weeks. Control mice were given same volume of corn oil. The liver and serum samples were collected after the last injection of CCl₄.

Figure 13. (See previous page). *Heg* deficiency in liver endothelial cells does not affect BDL-induced injury. A-G, H&E (A), Sirius red (B), desmin (C), and CK19 (D) staining and quantification (E-G) of sham group and BDL model at 1-, 2-, and 3-week time points show no difference in the injury severity between control and *Lyve1-Cre;Heg^{fl/fl}* livers. H, mRNA level of macrophage marker (F4/80), fibrosis markers (*Col1a1*, *Acta2*, *Desmin*, and *Timp*), and marker of ductal reaction (CK19) of liver tissues in sham group and BDL model mice. I, Serum level of liver enzymes (ALP/ALT/AST) and bilirubin (TBIL/DBIL/IBIL) of sham group and BDL model mice shows BDL causes sever liver injury, but there is no significant difference between control and *Lyve1-Cre;Heg^{fl/fl}* mice. Data are presented as mean \pm SD using unpaired Student *t* test. **P* < .05; ***P* < .01; ****P* < .001. NS, not significant. Scale bars represent 100 μ m in panels A, B, and D and 50 μ m in panel C.

For the TAA-induced liver injury model, 8-week old female littermate mice were administered 300 mg/L thiocetamide (Solarbio, China) via the drinking water for 8

weeks; control mice were given sterilized water, after which the liver and serum samples were collected for analysis.



For the acetaminophen (APAP)-induced acute liver injury, 8-week old male littermate mice were administered 300 mg/kg APAP (Aladdin, China) via oral gavage after 12 hours of starvation. Control mice were given same volume of PBS. Liver and serum samples were taken at 24 hours or 48 hours post-APAP treatment.

For the BDL model, 8-week old male mice were anesthetized with avertin and subjected to a mid-abdominal incision about 3 cm long, the common bile duct was ligated with 4-0 silk in 2 adjacent positions approximately 1 cm apart. The bile duct was then severed by incision between the two sites of ligation. Sham group was operated similarly, except that the bile duct was not ligated. Liver tissues and serum samples were collected at 1, 2, and 3 weeks after BDL.

For all the injury models, the body and liver weight of the mice were measured. After perfusion with PBS from the portal vein, the livers were fixed in 4% PFA overnight, dehydrated in 100% ethanol, and embedded in paraffin. Sections (6- μ m thick) were stained with H&E. Hepatic collagen contents were evaluated by Sirius red staining of paraffin-embedded sections. Liver function-related enzymes (ALT, AST, and ALP) and bilirubin (TBIL, direct bilirubin [DBIL], and indirect bilirubin [IBIL]) levels were measured by an automatic biochemical analyzer (AU5800, Beckman Colter Chemistry System analyzer).

TUNEL Staining

After dewaxing and hydration, tissue sections were boiled in 10-mM citrate buffer solution (pH 6.0) for antigen retrieval, then blocked with 10% donkey serum at room temperature, and incubated with appropriate primary antibodies overnight at 4°C. TUNEL was performed to detect apoptotic nuclei by using terminal deoxynucleotidyl transferase-mediated biotin-conjugated dUTP nick end labeling technique according to the manufacturer's protocol (Servicebio, China), nuclei were counterstained with hematoxylin.

Statistical Analysis

The data in this study are expressed as the mean \pm standard deviation (SD) or mean \pm standard error of the mean (SEM) as noted in individual figure legends. Statistical analyses were performed using GraphPad PRISM software, version 9.0. The unpaired Student *t* test were used to assess the differences between groups. Differences were considered statistically significant when $P < .05$, $P < .01$, or $P < .001$.

List of qPCR Primers

Acta2, Fwd 5'-TAGAACACGGCATCATCACCAA-3', Rev, 5-CAGAGTCCAGCACAATACCAGT-3';
Apc, Fwd 5'-CGAAAATGGGGTCCAAGGTA-3', Rev, 5-CGTAGTTTCACTCCGGGAAA-3';
Arg1, Fwd 5'-CGAAGCAAGCCAAGGTTAAAGCCAC-3', Rev, 5-GGAGGCCTATCTTACAGAGAAGGTC-3';
Axin2, Fwd 5'-CGGAAACAGCTGAAAACGGATT-3', Rev, 5-AGGTAGAGACACTTGGCCATTG-3';
 β -*Catenin*, Fwd 5'-AAGGAAGCTTCCAGACATGC-3', Rev, 5-AGCTTGCTCTCTTGATTGCC-3';
Ccnd1, Fwd 5'-CGGCCCAGGAGCTG-3', Rev, 5-GGCCAGGTTCCACTTGAGC-3';
Ces1b, Fwd 5'-AACGGCCAGTCTTCTCTTGAG-3', Rev, 5-CTGGGGTCTCTTGTCAGACAC-3';
Ces1d, Fwd 5'-CCCTCTTGGCTCCTTGAGATTT-3', Rev, 5-CCATCACTGGTAGTCTGCTGTT-3';
Ces1g, Fwd 5'-GCACACCACTTCCCTACCCTC-3', Rev, 5-AGGGCACTCCATCATAGGT-3';
Cyp1a2, Fwd 5'-ATCCTTTGTCCCCTTACCAT-3', Rev, 5-GGGAATGTGGAAGCCATTCA-3';
Cyp4a14, Fwd 5'-GTGCCTGCTTACAGTGTCTCT-3', Rev, 5-TGGAAGGCTGGAGTCAACATC-3';
Cyp4a32, Fwd 5'-TGCTAGACAAATGGGAAAGGCT-3', Rev, 5-ATCTGTGTGATCATGGGCAAGT-3';
Cyp7a1, Fwd 5'-CACCATTCTGCAACCTTCT-3', Rev, 5-TTGGCCAGCATCTGTAATG-3';
Cyp2e1, Fwd 5'-CACCGTGTCCGAGGATATGTCATC-3', Rev, 5-ACACACGCGCTTTCCTGCAGAAAAC-3';
Cyp2b9, Fwd 5'-CTCTGGCCACCATGAAAGAGT-3', Rev, 5-AGCAGATGATGTTGGCTGTGA-3';
Cyp2b10, Fwd 5'-CACGGAGTCCATCACCAGAA-3', Rev, 5-CTGTGTGGCACTCCAATAGGT-3';
Cyp2f2, Fwd 5'-TCGCTTCGACTATGACGATGAG-3', Rev, 5-TATTGAAGTGGCTCAGTGGGTC-3';
Col1a1, Fwd 5'-GCTCCTCTTAGGGCCACT-3', Rev, 5-ATTGGGGACCCTTAGGCCAT-3';
Cps1, Fwd 5'-TCTGTTGCTGGTGAAGTGGTT-3', Rev, 5-AGCCATTGACCCAGACTCTTG-3';
Ck19, Fwd 5'-GATCGTCTCGCCTCTACTTG-3', Rev, 5-CAGCGGAGCATTGTCAATCTG-3';
Ddr2, Fwd 5'-GGACATCACAGCCTCAAGTCA-3', Rev, 5-AATTCAATGCCATGACCCCT-3';
Desmin, Fwd 5'-GATAGACGACCTGCAGAGGC-3', Rev, 5-CATACTGAGCCCGGATGTCC-3';
Ecad, Fwd 5'-CAGTGAAGCGGCATCTAAAGC-3', Rev, 5-TTTTCATTTTCGGGGCAGCTG-3';
F4/80, Fwd 5'-TGACTCACCTTGTGGTCCTAA-3', Rev, 5-CTTCCCAGAATCCAGTCTTTCC-3';

Figure 14. (See previous page). *Heg* deficiency in liver endothelial cells protects the liver from APAP-induced acute liver injury. A, Metabolism process of acetaminophen and related enzymes. B, The expression levels of a list of reported enzymes involved in acetaminophen metabolism in the livers of control and *Lyve1-Cre;Heg^{fl/fl}* mice as measured by TPM values of RNA-seq. C, Serum liver enzyme analysis (ALT, AST, and ALP) indicate less acute damage to liver function in APAP treated 8-week *Lyve1-Cre;Heg^{fl/fl}* mice. D-E, H&E staining (D) and quantification (E) show less damaged area of pericentral hepatocytes in *Lyve1-Cre;Heg^{fl/fl}* mice 24 hours post APAP treatment. F-G, TUNEL staining (F) and quantification (G) show less cell death of pericentral hepatocytes in *Lyve1-Cre;Heg^{fl/fl}* mice 24 hours post APAP treatment. Data are presented as mean \pm SD using unpaired Student *t* test ($n = 4$ pair for sham group and $n = 4$ pair for APAP group), * $P < .05$; *** $P < .001$. Scale bars represent 100 μ m in panels B and C.

Fzd4, Fwd 5'-TCCAGCCAGCTGCAGTTC-3', Rev, 5-TTGTGGTCTGTTCTGGGGC-3';
Fzd5, Fwd 5'-CACAGGTACCTAGCTTGTGTT-3', Rev, 5-GCACTCAGTTCCACACCAGATA-3';
Fzd6, Fwd 5'-GCCGGAACCAAGAGAAGCT-3', Rev, 5-TTCCAACCCAGAAGACCGC-3';
Gls2, Fwd 5'-GGAGCGTATCCCTATCCACAAG-3', Rev, 5-CGTGAACTCCTCAAAGTCAGGA-3';
Gul1, Fwd 5'-GCCAGGAGAAGAAGGGCTACTTTGA-3', Rev, 5-GAGAGGGATCACTGGAAGTCTAGTC-3';
Hsd17, Fwd 5'-TAGTGCCAAGGACGAGGAGA-3', Rev, 5-GCAGAGACACGAGGTTTGA-3';
IL1b, Fwd 5'-TGTAATGAAAGACGGCACACC-3', Rev, 5-TCTTCTTTGGGTATTGCTTGG-3';
IL6, Fwd 5'-CAAAGCCAGATCCTTCAGA-3', Rev, 5-GATGGTCTTGGTCCTTAGCC-3';
Lgr4, Fwd 5'-CGCCTTACCCAAGCACTA-3', Rev, 5-AGATGCCGCAACTGAACGA-3';
Oat, Fwd 5'-CAATTACCATCCTTTGCCTGTA-3', Rev, 5-GTACTGCCTGCCTTCCACAT-3';
Rdh9, Fwd 5'-AGAGGCATGAGAGTGTGGC-3', Rev, 5-CTCGATCAAGCCCAACAGGT-3';
Rnf43, Fwd 5'-AAGCTAATGCAGTCCCACCC-3', Rev, 5-CAGCACCCTGGCTTAGTCA-3';
Rspo3, Fwd 5'-GGGGGACTGAAACACGGG-3', Rev, 5-GCTGCTGCTGCCTCTCTT-3';
Tgfβ, Fwd 5'-CTCCGTGGCTTCTAGTGC-3', Rev, 5-GCCTTAGTTTGGACAGGATCTG-3';
Timp1, Fwd 5'-CTTGTTCCCTGGCGTACTC-3', Rev, 5-ACCTGATCCGTCCACAAACAG-3';
Wnt2, Fwd 5'-CCTGATGAACCTTACAACAAC-3', Rev, 5-TCTTGTTCAGAAGCGCTTTAC-3';
Wnt9b, Fwd 5'-CTGGTGCTCACCTGAAGCAG-3', Rev, 5-CCGTCTCCTTAAAGCCTCTCTG-3';
Znf3, Fwd 5'-TCCAGCACCTCCCTCCTC-3', Rev, 5-CGCTGCTCAGTGTGTTCCA-3'.

References

1. Teutsch HF. The modular microarchitecture of human liver. *Hepatology* 2005;42:317–325.
2. Sparks EE, Perrien DS, Huppert KA, Peterson TE, Huppert SS. Defects in hepatic Notch signaling result in disruption of the communicating intrahepatic bile duct network in mice. *Dis Model Mech* 2011;4:359–367.
3. Tanimizu N, Kaneko K, Itoh T, Ichinohe N, Ishii M, Mizuguchi T, Hirata K, Miyajima A, Mitaka T. Intrahepatic bile ducts are developed through formation of homogeneous continuous luminal network and its dynamic rearrangement in mice. *Hepatology* 2016;64:175–188.
4. Dimri M, Bilogan C, Pierce LX, Naegel G, Vasanthi A, Gibson I, McClendon A, Tae K, Sakaguchi TF. Three-dimensional structural analysis reveals a Cdk5-mediated kinase cascade regulating hepatic biliary network branching in zebrafish. *Development* 2017;144:2595–2605.
5. Hikspoors J, Peeters M, Kruepunga N, Mekonen HK, Mommens GMC, Kohler SE, Lamers WH. Human liver segments: role of cryptic liver lobes and vascular physiology in the development of liver veins and left-right asymmetry. *Sci Rep* 2017;7:17109.
6. Preziosi M, Okabe H, Poddar M, Singh S, Monga SP. Endothelial Wnts regulate beta-catenin signaling in murine liver zonation and regeneration: a sequel to the Wnt-Wnt situation. *Hepatol Commun* 2018;2:845–860.
7. Leibing T, Geraud C, Augustin I, Boutros M, Augustin HG, Okun JG, Langhans CD, Zierow J, Wohlfeil SA, Olsavszky V, Schledzewski K, Goerdts S, Koch PS. Angiocrine Wnt signaling controls liver growth and metabolic maturation in mice. *Hepatology* 2018;68:707–722.
8. Ben-Moshe S, Itzkovitz S. Spatial heterogeneity in the mammalian liver. *Nature Rev Gastroenterol Hepatol* 2019;16:395–410.
9. Gebhardt R, Matz-Soja M. Liver zonation: novel aspects of its regulation and its impact on homeostasis. *World J Gastroenterol* 2014;20:8491–8504.
10. Jungermann K, Kietzmann T. Zonation of parenchymal and nonparenchymal metabolism in liver. *Annu Rev Nutr* 1996;16:179–203.
11. Rocha AS, Vidal V, Mertz M, Kendall TJ, Charlet A, Okamoto H, Schedl A. The angiocrine factor rspondin3 is a key determinant of liver zonation. *Cell Rep* 2015;13:1757–1764.
12. Planas-Paz L, Orsini V, Boulter L, Calabrese D, Pikiolk M, Nigsch F, Xie Y, Roma G, Donovan A, Marti P, Beckmann N, Dill MT, Carbone W, Bergling S, Isken A, Mueller M, Kinzel B, Yang Y, Mao X, Nicholson TB, Zamponi R, Capodici P, Valdez R, Rivera D, Loew A, Ukomadu C, Terracciano LM, Bouwmeester T, Cong F, Heim MH, Forbes SJ, Ruffner H, Tchorz JS. The RSPO-LGR4/5-ZNRF3/RNF43 module controls liver zonation and size. *Nat Cell Biol* 2016;18:467–479.
13. Ma R, Martinez-Ramirez AS, Borders TL, Gao F, Sosa-Pineda B. Metabolic and non-metabolic liver zonation is established non-synchronously and requires sinusoidal Wnts. *eLife* 2020;9:e46206.
14. Kohle C, Bock KW. Coordinate regulation of human drug-metabolizing enzymes, and conjugate transporters by the Ah receptor, pregnane X receptor and constitutive androstane receptor. *Biochem Pharmacol* 2009;77:689–699.
15. Braeuning A, Sanna R, Huelsken J, Schwarz M. Inducibility of drug-metabolizing enzymes by xenobiotics in mice with liver-specific knockout of Ctnnb1. *Drug Metab Dispos* 2009;37:1138–1145.
16. Kleaveland B, Zheng X, Liu JJ, Blum Y, Tung JJ, Zou Z, Sweeney SM, Chen M, Guo L, Lu MM, Zhou D, Kitajewski J, Affolter M, Ginsberg MH, Kahn ML. Regulation of cardiovascular development and integrity by the heart of glass-cerebral cavernous malformation protein pathway. *Nat Med* 2009;15:169–176.
17. Sakaguchi TF, Sadler KC, Crosnier C, Stainier DY. Endothelial signals modulate hepatocyte apical polarization in zebrafish. *Curr Biol* 2008;18:1565–1571.
18. Mably JD, Mohideen MA, Burns CG, Chen JN, Fishman MC. Heart of glass regulates the concentric growth of the heart in zebrafish. *Curr Biol* 2003;13:2138–2147.

19. Tabula Muris Consortium. Single-cell transcriptomics of 20 mouse organs creates a Tabula Muris. *Nature* 2018; 562:367–372.
20. Raynaud P, Carpentier R, Antoniou A, Lemaigre FP. Biliary differentiation and bile duct morphogenesis in development and disease. *Int J Biochem Cell Biol* 2011; 43:245–256.
21. Liu Y, Meyer C, Xu C, Weng H, Hellerbrand C, ten Dijke P, Dooley S. Animal models of chronic liver diseases. *Am J Physiol Gastrointest Liver Physiol* 2013; 304:G449–G468.
22. Maes M, Vinken M, Jaeschke H. Experimental models of hepatotoxicity related to acute liver failure. *Toxicol Appl Pharmacol* 2016;290:86–97.
23. Wallace MC, Hamesch K, Lunova M, Kim Y, Weiskirchen R, Strnad P, Friedman SL. Standard operating procedures in experimental liver research: thioacetamide model in mice and rats. *Lab Anim* 2015; 49(1 Suppl):21–29.
24. Bernal W, Wendon J. Acute liver failure. *N Engl J Med* 2013;369:2525–2534.
25. Mossanen JC, Tacke F. Acetaminophen-induced acute liver injury in mice. *Lab Anim* 2015;49(1 Suppl):30–36.
26. Sparks EE, Huppert KA, Brown MA, Washington MK, Huppert SS. Notch signaling regulates formation of the three-dimensional architecture of intrahepatic bile ducts in mice. *Hepatology* 2010;51:1391–1400.
27. Collardeau-Frachon S, Scoazec JY. Vascular development and differentiation during human liver organogenesis. *Anat Rec (Hoboken)* 2008;291:614–627.
28. Tanimizu N, Miyajima A. Molecular mechanism of liver development and regeneration. *Int Rev Cytol* 2007; 259:1–48.
29. Lemaigre FP. Development of the intrahepatic and extrahepatic biliary tract: a framework for understanding congenital diseases. *Annu Rev Pathol* 2020;15:1–22.
30. Hofmann JJ, Zovein AC, Koh H, Radtke F, Weinmaster G, Iruela-Arispe ML. Jagged1 in the portal vein mesenchyme regulates intrahepatic bile duct development: insights into Alagille syndrome. *Development* 2010;137:4061–4072.
31. Matsumoto K, Yoshitomi H, Rossant J, Zaret KS. Liver organogenesis promoted by endothelial cells prior to vascular function. *Science* 2001;294:559–563.
32. Field HA, Ober EA, Roeser T, Stainier DY. Formation of the digestive system in zebrafish. I. Liver morphogenesis. *Dev Biol* 2003;253:279–290.
33. Valle-Encinas E, Dale TC. Wnt ligand and receptor patterning in the liver. *Curr Opin Cell Biol* 2020;62:17–25.
34. Benhamouche S, Decaens T, Godard C, Chambrey R, Rickman DS, Moinard C, Vasseur-Cognet M, Kuo CJ, Kahn A, Perret C, Colnot S. Apc tumor suppressor gene is the “zonation-keeper” of mouse liver. *Dev Cell* 2006; 10:759–770.
35. Yang J, Mowry LE, Nejak-Bowen KN, Okabe H, Diegel CR, Lang RA, Williams BO, Monga SP. beta-catenin signaling in murine liver zonation and regeneration: a Wnt-Wnt situation. *Hepatology* 2014;60:964–976.
36. Tan X, Behari J, Cieply B, Michalopoulos GK, Monga SP. Conditional deletion of beta-catenin reveals its role in liver growth and regeneration. *Gastroenterology* 2006; 131:1561–1572.
37. Wang B, Zhao L, Fish M, Logan CY, Nusse R. Self-renewing diploid Axin2(+) cells fuel homeostatic renewal of the liver. *Nature* 2015;524:180–185.
38. Mak KM, Png CYM. The hepatic central vein: structure, fibrosis, and role in liver biology. *Anat Rec (Hoboken)* 2020;303:1747–1767.
39. Sekine S, Lan BY, Bedolli M, Feng S, Hebrok M. Liver-specific loss of beta-catenin blocks glutamine synthesis pathway activity and cytochrome p450 expression in mice. *Hepatology* 2006;43:817–825.
40. Scholten D, Trebicka J, Liedtke C, Weiskirchen R. The carbon tetrachloride model in mice. *Lab Anim* 2015;49(1 Suppl):4–11.
41. Dhaliwal HS, Singh P. Acute liver failure. *N Engl J Med* 2014;370:1170.
42. Yan M, Huo Y, Yin S, Hu H. Mechanisms of acetaminophen-induced liver injury and its implications for therapeutic interventions. *Redox Biol* 2018;17:274–283.
43. de Kreuk BJ, Gingras AR, Knight JD, Liu JJ, Gingras AC, Ginsberg MH. Heart of glass anchors Rasip1 at endothelial cell-cell junctions to support vascular integrity. *eLife* 2016;5:e11394.
44. Koo Y, Barry DM, Xu K, Tanigaki K, Davis GE, Mineo C, Cleaver O. Rasip1 is essential to blood vessel stability and angiogenic blood vessel growth. *Angiogenesis* 2016;19:173–190.
45. Wustehube J, Bartol A, Liebler SS, Brutsch R, Zhu Y, Felbor U, Sure U, Augustin HG, Fischer A. Cerebral cavernous malformation protein CCM1 inhibits sprouting angiogenesis by activating DELTA-NOTCH signaling. *Proc Natl Acad Sci U S A* 2010;107:12640–12645.
46. Scholz B, Korn C, Wojtarowicz J, Mogler C, Augustin I, Boutros M, Niehrs C, Augustin HG. Endothelial RSP03 controls vascular stability and pruning through non-canonical WNT/Ca(2+)/NFAT signaling. *Dev Cell* 2016; 36:79–93.
47. Heinke J, Wehofsits L, Zhou Q, Zoeller C, Baar KM, Helbing T, Laib A, Augustin H, Bode C, Patterson C, Moser M. BMPER is an endothelial cell regulator and controls bone morphogenetic protein-4-dependent angiogenesis. *Circ Res* 2008;103:804–812.
48. Li GX, Zhang S, Liu R, Singh B, Singh S, Quinn DI, Crump G, Gill PS. Tetraspanin18 regulates angiogenesis through VEGFR2 and Notch pathways. *Biol Open* 2021; 10:bio050096.
49. Zhao YR, Wang JL, Xu C, Li YM, Sun B, Yang LY. HEG1 indicates poor prognosis and promotes hepatocellular carcinoma invasion, metastasis, and EMT by activating Wnt/beta-catenin signaling. *Clin Sci (Lond)* 2019;133:1645–1662.
50. National Research Council (US) Committee for the Update of the Guide for the Care and Use of Laboratory Animals. *Guide for the Care and Use of Laboratory Animals*. Washington (DC); 2011.
51. Kaneko K, Kamimoto K, Miyajima A, Itoh T. Adaptive remodeling of the biliary architecture underlies liver homeostasis. *Hepatology* 2015;61:2056–2066.
52. Duan JL, Ruan B, Yan XC, Liang L, Song P, Yang ZY, Liu Y, Dou KF, Han H, Wang L. Endothelial Notch

activation reshapes the angiocrine of sinusoidal endothelia to aggravate liver fibrosis and blunt regeneration in mice. *Hepatology* 2018;68:677–690.

53. Perteu M, Perteu GM, Antonescu CM, Chang TC, Mendell JT, Salzberg SL. StringTie enables improved reconstruction of a transcriptome from RNA-seq reads. *Nat Biotechnol* 2015;33:290–295.

Renhua Song (Formal analysis: Equal; Investigation: Supporting; Methodology: Supporting; Validation: Supporting; Visualization: Supporting; Writing – review & editing: Supporting)

Huilii Yan (Data curation: Supporting; Methodology: Supporting; Validation: Supporting)

Xi Yang (Data curation: Supporting; Methodology: Supporting; Resources: Supporting)

Junhao Hu (Methodology: Supporting; Writing – review & editing: Supporting)

Xiaohong Wang (Data curation: Supporting; Formal analysis: Supporting; Validation: Supporting)

Zhiming Han (Data curation: Supporting; Formal analysis: Supporting; Validation: Supporting; Writing – review & editing: Supporting)

Yi Zhu (Methodology: Supporting; Resources: Supporting; Validation: Supporting)

Renjing Liu (Formal analysis: Supporting; Validation: Supporting; Writing – original draft: Supporting; Writing – review & editing: Equal)

Justin Wong (Formal analysis: Supporting; Investigation: Supporting; Methodology: Supporting; Supervision: Supporting; Validation: Supporting; Writing – review & editing: Supporting)

Geoffrey McCaughan (Formal analysis: Supporting; Methodology: Supporting; Supervision: Supporting; Validation: Supporting; Writing – original draft: Supporting; Writing – review & editing: Supporting)

Xiangjian Zheng (Conceptualization: Lead; Data curation: Supporting; Formal analysis: Lead; Funding acquisition: Lead; Investigation: Lead; Methodology: Equal; Project administration: Lead; Resources: Lead; Supervision: Lead; Validation: Equal; Visualization: Equal; Writing – original draft: Lead; Writing – review & editing: Lead)

Received August 4, 2021. Accepted February 14, 2022.

Correspondence

Address correspondence to: Dr Xiangjian Zheng, Pharmacology, Tianjin Medical University, No 22 Qi Xiang Tai Rd, Tianjin 300070, China. e-mail: xzheng@tmu.edu.cn. tel: 86-22-8333-6835.

Acknowledgment

The authors thank Dr. Mark Kahn for the generous gifts of *Heg*^{-/-} and *Heg*^{fl/m} mice. The authors thank Jisheng Yang and Li Li for the advices on histology techniques and Ziran Xu for the help with RNAscope analysis.

CRediT Authorship Contributions

Shichao Zhu (Conceptualization: Supporting; Data curation: Lead; Formal analysis: Lead; Investigation: Lead; Methodology: Lead; Validation: Equal; Visualization: Equal; Writing – original draft: Equal; Writing – review & editing: Equal)

Xiyun Rao (Data curation: Supporting; Formal analysis: Supporting; Investigation: Supporting; Methodology: Supporting; Validation: Supporting; Visualization: Supporting; Writing – original draft: Supporting; Writing – review & editing: Supporting)

Yude Qian (Data curation: Supporting; Investigation: Supporting; Methodology: Supporting; Validation: Supporting; Visualization: Supporting; Writing – review & editing: Supporting)

Jinbiao Chen (Data curation: Supporting; Formal analysis: Supporting; Investigation: Supporting; Methodology: Supporting; Validation: Supporting; Writing – original draft: Supporting; Writing – review & editing: Supporting)

Conflicts of interest

The authors disclose no conflicts.

Funding

The project is supported by funding from National Key Research and Development Program of China (grants 2019YFA0802003 to Xiangjian Zheng), National Natural Science Foundation of China grants 81771240 (Xiangjian Zheng), Australian National Heart Foundation Future Leader Fellowship (101856), and National Health and Medical Research Council (1158997, 1158998) (Renjing Liu).